NAVAL POSTGRADUATE SCHOOL
Monterey, California

THESIS

PHOTOELASTIC STUDY OF ELASTIC AND PLASTIC STRESS FIELDS IN THE VICINITY OF A NOTCH

by

Frank E. Stenstrom

December 1980

Thesis Advisor: G. H. Lindsey

Approved for public release; distribution unlimited

REPORT DOCUMENTATION PAGE

READ INSTRUCTIONS BEFORE COMPLETING FORM

1. REPORT NUMBER	2. GOVT ACCESSION NO. / 3. RECIPIENT'S CATALOG NUMBER
4. TITLE (and Subtitle): Photoelastic Study of Elastic and Plastic Stress Fields in the Vicinity of a Notch	5. TYPE OF REPORT & PERIOD COVERED: Master's Thesis; December 1980
	6. PERFORMING ORG. REPORT NUMBER
7. AUTHOR(s): Frank E. Stenstrom	8. CONTRACT OR GRANT NUMBER(s)
9. PERFORMING ORGANIZATION NAME AND ADDRESS: Naval Postgraduate School, Monterey, California 93940	10. PROGRAM ELEMENT, PROJECT, TASK AREA & WORK UNIT NUMBERS
11. CONTROLLING OFFICE NAME AND ADDRESS: Naval Postgraduate School, Monterey, California 93940	12. REPORT DATE: December 1980
	13. NUMBER OF PAGES: 84 pages
14. MONITORING AGENCY NAME & ADDRESS (if different from Controlling Office): Naval Postgraduate School, Monterey, California 93940	15. SECURITY CLASS. (of this report): Unclassified
	15a. DECLASSIFICATION/DOWNGRADING SCHEDULE

16. DISTRIBUTION STATEMENT (of this Report)
Approved for public release; distribution unlimited

17. DISTRIBUTION STATEMENT (of the abstract entered in Block 20, if different from Report)

18. SUPPLEMENTARY NOTES

19. KEY WORDS (Continue on reverse side if necessary and identify by block number)
Photoelastic, Stress, Strain, Stress Concentration Factor, Residual Stress, Notch, Plastic Zone

20. ABSTRACT (Continue on reverse side if necessary and identify by block number)
The ability to calculate stresses in critical areas by measuring strains at far-field locations will be essential to the success of new fatigue monitoring equipment currently being developed. In this thesis the photoelastic method was utilized to study plastic zone characteristics and residual compressive stresses in critical areas modeled by notched specimens. Data reduction methods for photoelastic measurements were developed by a thorough investigation of reinforcement effects and by a careful

Item 20

determination of material properties of PS-1C Photoelastic Material and 7075-T6 aluminum. A modified Ramberg-Osgood data reduction method was developed for determining stresses from strains measured in the plastic region. Stresses obtained from slip-line theory for rigid-perfectly-plastic material were compared to the experimental results, and differences noted. Notch tip stresses and strains were compared to predictions using Neuber's relation. The measured data indicated stress concentrations 20.9% lower than predicted by Neuber.

Approved for public release; distribution unlimited

PHOTOELASTIC STUDY OF ELASTIC AND PLASTIC STRESS FIELDS IN THE VICINITY OF A NOTCH

by

Frank E. Stenstrom
Lieutenant Commander, United States Navy
B.S., United States Naval Academy, 1969

Submitted in partial fulfillment of the
requirements for the degree of

MASTER OF SCIENCE IN AERONAUTICAL ENGINEERING

from the

NAVAL POSTGRADUATE SCHOOL
December 1980

ABSTRACT

The ability to calculate stresses in critical areas by measuring strains at far-field locations will be essential to the success of new fatigue monitoring equipment currently being developed. In this thesis the photoelastic method was utilized to study plastic zone characteristics and residual compressive stresses in critical areas modeled by notched specimens. Data reduction methods for photoelastic measurements were developed by a thorough investigation of reinforcement effects and by a careful determination of material properties of PS-1C Photoelastic Material and 7075-T6 aluminum. A modified Ramberg-Osgood data reduction method was developed for determining stresses from strains measured in the plastic region. Stresses obtained from slip-line theory for rigid-perfectly-plastic material were compared to the experimental results, and differences noted. Notch tip stresses and strains were compared to predictions using Neuber's relation. The measured data indicated stress concentrations 20.9% lower than predicted by Neuber.

TABLE OF CONTENTS

LIST OF FIGURES

ACKNOWLEDGEMENT

I would like to express my sincere appreciation for the patience and guidance of Professor G. H. Lindsey in planning the experimental work and providing valuable assistance in completing this thesis. Mr. Bob Besel and his staff are to be commended for outstanding support.

I. INTRODUCTION

Modern Naval aircraft instruments are capable of recording several types of data in flight among which is the capability to measure nominal strains near fatigue critical areas during maneuvers. Due to gage fatigue limitations it is not possible to mount strain gages right at the critical areas, and it becomes important, therefore, to understand the relationship between a nominal, far-field strain measurement and the local strain at the critical subject area. Previous methods have utilized Neuber's relationship [Ref. 1], which could have significant error at low strain levels as shown by Garske in Ref. 2. Furthermore, several investigators have shown that if a sufficient stress concentration is introduced to produce a plastic zone around a notch, the unloading of the material will produce a residual compressive stress around the notch tip and increase the fatigue life of the material [Refs. 3, 4, 5].

An experimental investigation was undertaken to statically load flat plate notched specimens, which simulated wing skins or other aircraft structure containing stress concentrations. Photoelastic measurements were made in the vicinity of the notch to study the elastic stress distribution, the plastic yield zone and the residual compressive stresses remaining after unloading. Initial phases of the work included a

complete characterization of the photoelastic material, a detailed analysis of unbound effects, evaluation of the Poisson's ratio mismatch, and the effects of reinforcement of the specimen by the bonded photoelastic material. A modified Ramberg-Osgood method was used to reduce biaxial strains to stresses in the plastic regions. Stresses in the plastic zone were compared to classical plane stress slip-line theory and Neuber's relation was evaluated using the plastic zone stress and strain concentration factors.

II. CHARACTERIZATION OF PS-1C PHOTOELASTIC MATERIAL

Two uniaxial tensile test specimens were prepared from a single sheet of PS-1C Photoelastic Material. The first specimen was 1.0 inch wide and was used for thickness measurement, longitudinal strain data, and was eventually bonded to an aluminum test specimen. The second 2.0 inch wide specimen was used for transverse strain data and for measuring photoelastic coating fringe value, F_σ.

A. THICKNESS DETERMINATION

One longitudinal edge of the 1.0 inch wide specimen was lightly sanded to create a smooth, uniform cross-section of the photoelastic material. The specimen was then mounted such that a traveling microscope could be used to measure thickness. With the capability of measuring thickness and the contrast in appearance between the reflective coating and the base material, it was possible to accurately determine the thickness of both. For the specimen viewed, the base thickness was measured to be 0.0382 inches and the reflective coating to be 0.0051 inches. These numbers were obtained by measuring eight separate points along the edge and averaging the results. The total thickness of 0.0433 inches fell within the range of the advertised 0.044 ± 0.002 inches. It was, therefore, concluded that the labeled

thickness included both the base and the reflective coating after two similar specimens of different marked thicknesses were checked. For calculation purposes, the thickness of the original specimen was taken to be 0.0382 inches since the path of polarized light does not penetrate the reflective coating of the photoelastic material, and it was assumed that the reflective coating does not contribute to the strength of nor does it reinforce the base material.

B. YOUNG'S MODULUS

Two lines were lightly etched on the surface of the 1.0 inch wide specimen in the horizontal direction in order to accommodate a Tuckerman Optical Strain Gage. The specimen was then loaded in tension. The readings taken with an auto-collimater were recorded in Table I (all tables are in Appendix A). Using American Instrument Company calibration factors, the strain was calculated with the following formula taken from Ref. 6.

$$S = \frac{F\ A\ L\ R}{1000e}$$

where S = Strain in micro inches per inch

F = Lozenge calibration factor, 1.002

A = Auto-collimater calibration factor, 1.004

L = Lozenge length, 2.0 inches

R = Net reading

e = Gage length, 1.0 inch

With the measured strain, the measured load at each point and the known cross-sectional area, Young's Modulus, E, was determined from the slope of the stress-strain curve shown in Figure 1, using a linear regression analysis.

$$\sigma = 357079.18\varepsilon_1 - 4.3407$$

$$R = .9988$$

where R = correlation coefficient.

Dropping the non-zero intercept, Young's modulus was taken to be 357,079.18 psi. Photolastic Inc. information shows this number to be nominally 360,000 psi. Using thin specimens, such as the photoelastic material, requires very accurate thickness measurements because E is directly proportional to thickness.

C. POISSON'S RATIO

Using the 2.0 inch wide PS-1C specimen, two lines were lightly etched into the surface in the longitudinal direction one inch apart. With the Tuckerman Optical Strain Gage mounted in the transverse direction as shown in Figure 2, the specimen was loaded in tension. The data points from Table I were used in a linear regression analysis with the following results:

$$\sigma = -941487.02\varepsilon_2 - 1.00708$$

$$R = .99991$$

Poisson's ratio was then determined by dropping the non-zero intercept and dividing the negative of the slope by E as

indicated in Figure 1. The measured Poisson's ratio is 0.37927 which compares with a nominal value of 0.38 supplied by Photolastic Inc.

D. COATING FRINGE VALUE IN TERMS OF STRESS, F_σ

Prior to etching lines on the 2.0 inch wide specimen, it was loaded in tension in the elastic region, and the fringe number, N, was determined using a reflection polariscope. With several load points and known dimensions, the stress was calculated and plotted against the fringe number. Using the data from Table II, a linear regression analysis yielded

$\sigma = 456.6661N+1.92740$

$R = .99932$

Dropping the non-zero intercept, F_σ was taken to be 456.67 psi/fringe.

PS-1C CHARACTERIZATION
STRESS-STRAIN CURVE

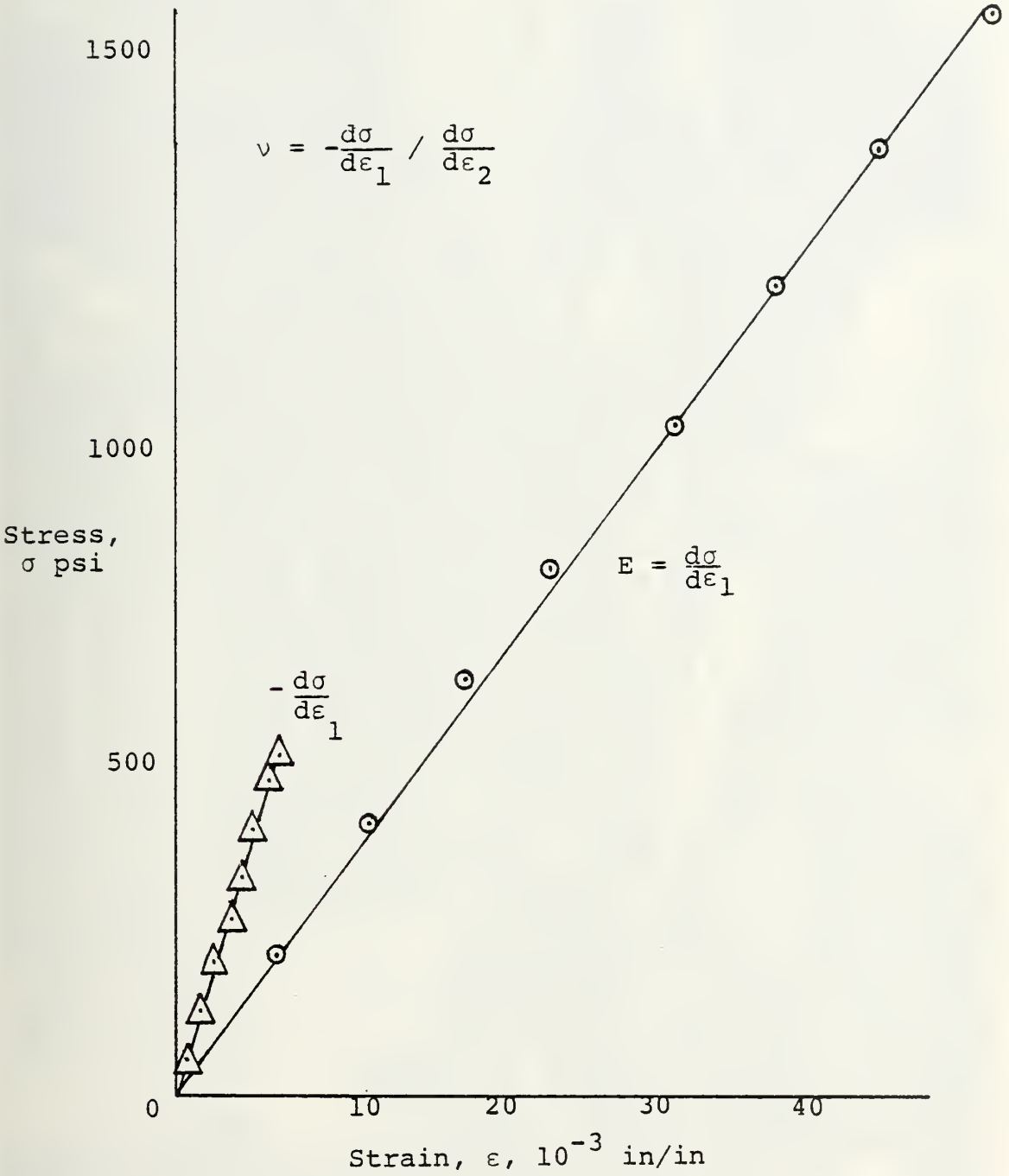

Figure 1

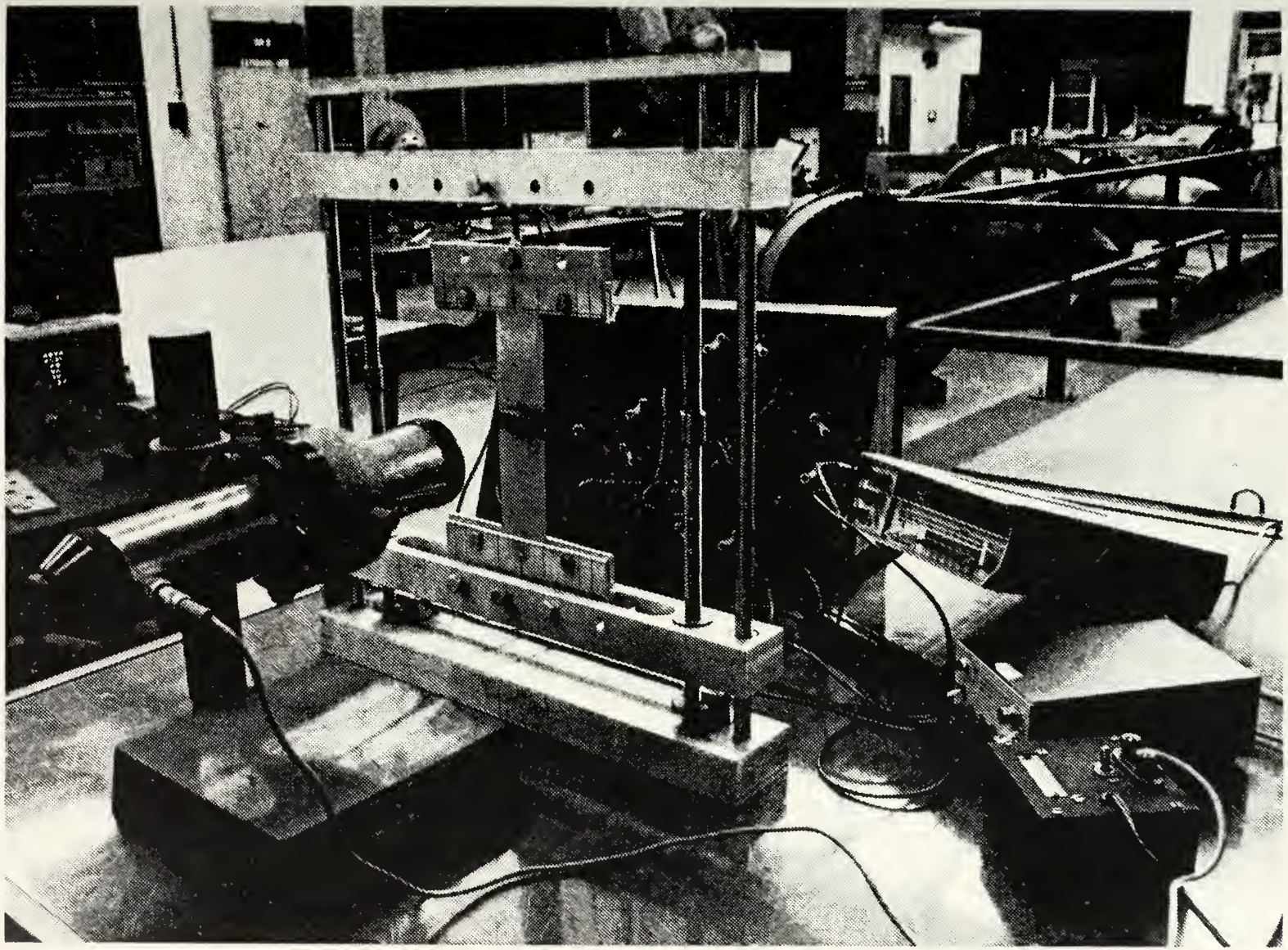

Figure 2. TUCKERMAN OPTICAL STRAIN GAGE SET-UP

III. CHARACTERIZATION OF 7075-T6 ALUMINUM

This characterization was performed on a uniaxial tensile test specimen of 7075-T6 aluminum to establish material properties for use in analytically deriving correction factors for a bonded specimen. Although nominal material properties were readily available from several sources, the ultimate desire was for superior accuracy of measured data.

A. YOUNG'S MODULUS

A rossette type strain gage was bonded to the aluminum specimen shown in Figure 3. The specimen was then mounted in a RIEHLE Test Machine with only transverse and longitudinal leads connected to a Switching and Balancing Unit. Readings were taken on an SR-4 Strain Indicator at the points shown in Table III. Width and thickness measurements were made with a micrometer. With the dimensions of the cross-section and with measured loads, stresses were calculated and plotted against strain. The slope of the resulting linear relation was determined by linear regression.

$$\sigma = 10.41518 \times 10^{6} \varepsilon_1 + 242.076$$

$$R = .99992$$

Dropping the non-zero intercept, Young's Modulus was taken to be 10.42×10^{6} psi for the unbonded aluminum specimen.

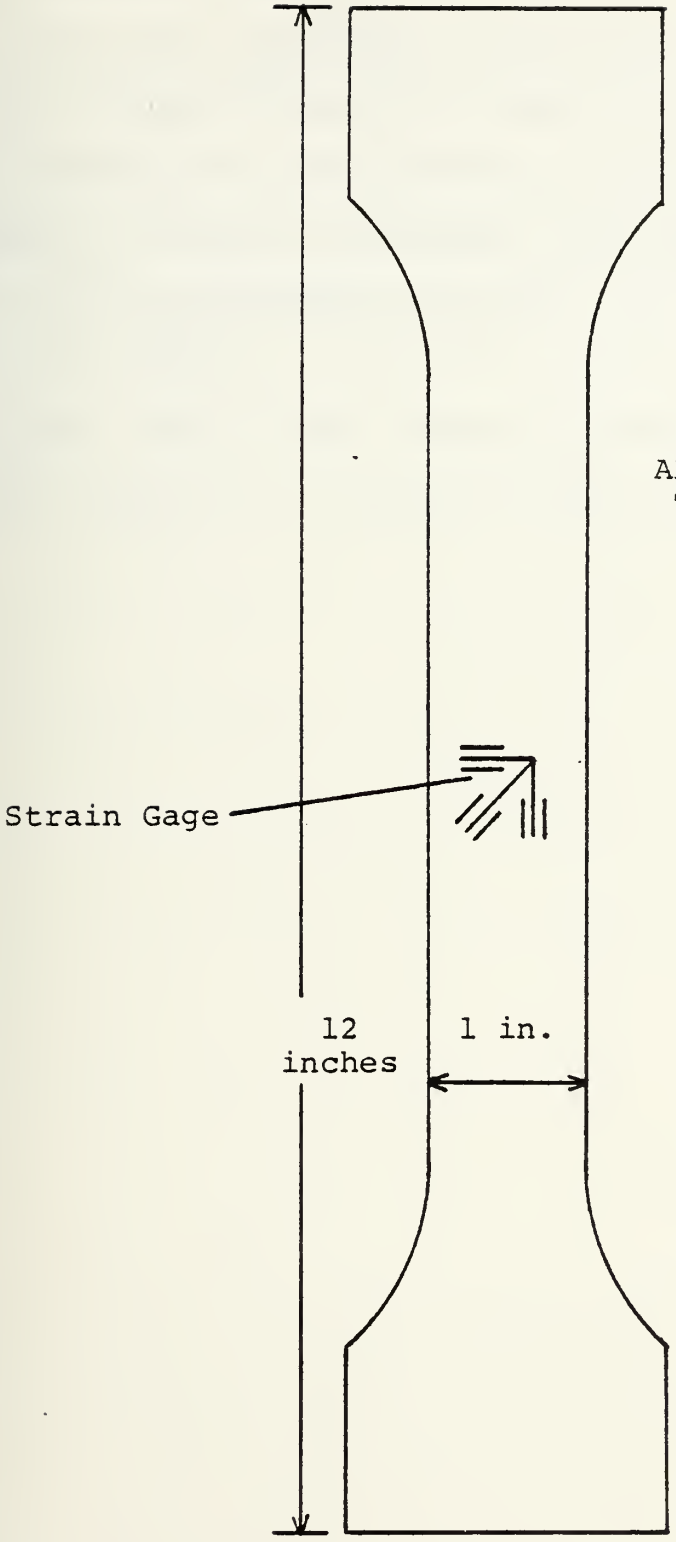

Figure 3

B. POISSON'S RATIO

Using the transverse strain data from Table III and Young's Modulus determined above, Poisson's ratio was found by dividing E by the negative of the transverse slope, the same as in the PS-1C analysis. By linear regression

$$\sigma = 32.19308 \times 10^{6} \varepsilon_2 + 172.365$$

$$R = .999927$$

Dropping the non-zero intercept and proceeding as described above results in a Poisson's ratio of 0.32352.

IV. REINFORCEMENT EFFECT OF BONDED PHOTOELASTIC MATERIAL

Photoelastic material bonded to a specimen becomes, in effect, an extension of the specimen itself and consequently modifies certain material properties of the specimen. Error exists in the use of photoelastic data without accounting for these changes. This section will explore the effect on Young's Modulus and Poisson's ratio from the free boundary of a specimen to the fully reinforced interior regions. A correction factor for interior points will be obtained.

A. YOUNG'S MODULUS MODEL

A model uniaxial bar with cross-sectional area, A^*, stress, σ^*, Young's Modulus, E^*, and strain, ε^*, is introduced. This model is the combination described in Figure 4 where

$$A^* = A_c + A_s \tag{1}$$

and

$$P = P_c + P_s \tag{2}$$

A^* = total cross-sectional area

A_c = coating cross-sectional area

A_s = specimen cross-sectional area

P = total load

P_c = load in the coating

P_s = load in the specimen

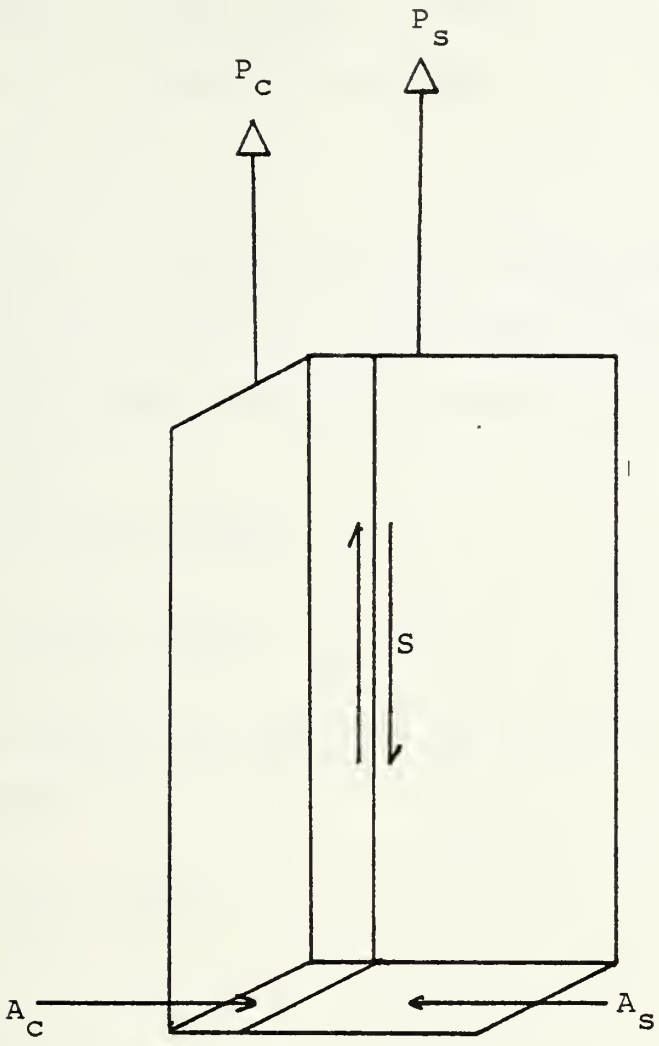

Sign Convention

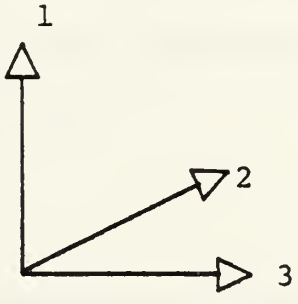

MODEL UNIAXIAL BAR

Figure 4

To develop a model Young's Modulus which reflects the properties of a reinforced specimen, the basic equation

$$\sigma^* = \frac{P}{A^*} \tag{3}$$

is introduced. If the strain in the specimen equals that in the coating, it follows that the model strain, ε^*, will also equal the other two. With the relation

$$\sigma^* = E^*\varepsilon^*, \tag{4}$$

it follows from (2) that

$$\sigma^*A^* = \sigma_c A_c + \sigma_s A_s. \tag{5}$$

Since the strains are equal in the model, the coating, and the specimen

$$\sigma_c = E_c\varepsilon_c = E_c\varepsilon^* \tag{6}$$

and

$$\sigma_s = E_s\varepsilon_s = E_s\varepsilon^* \tag{7}$$

If equations (6) and (7) are substituted back into (5) and ε^* cancelled, it follows that

$$E^* = \frac{E_c A_c + E_s A_s}{A^*} \tag{8}$$

At this point all the quantities on the right side of equation (8) are known. E^* is calculated to be 9.083×10^6 psi using previously measured values.

B. MODEL POISSON'S RATIO

To obtain a model quantity which reflects the Poisson effect of the combination of the specimen and bonded material, the basic definition of Poisson's ratio, ν, is recalled where

$$\varepsilon_2^* = \nu^* \varepsilon_1^*, \quad \varepsilon_{2c} = -\nu_c \varepsilon_{1c}, \quad \varepsilon_{2s} = -\nu_s \varepsilon_{1s} \tag{9}$$

and the relationship

$$\varepsilon_1^* = \frac{\sigma^*}{E^*}, \quad \varepsilon_{1c} = \frac{\sigma_c}{E_c}, \quad \varepsilon_{1s} = \frac{\sigma_s}{E_s} \tag{10}$$

where the 1 and 2 directions are those indicated in Figure 4. It follows that

$$\varepsilon_{2s} = -\nu_s \varepsilon_{1s} = -\frac{\nu_s \sigma_{1s}}{E_s} \tag{11}$$

and

$$\varepsilon_{2c} = -\nu_c \varepsilon_{1c} = -\frac{\nu_c \sigma_{1c}}{E_c} . \tag{12}$$

By solving for stress in equations (11) and (12) and substituting into (5),

$$\frac{-E^* \varepsilon_2^* A^*}{\nu^*} = -\frac{E_s \varepsilon_{2s} A_s}{\nu_s} - \frac{E_c \varepsilon_{2c} A_c}{\nu_c} \tag{13}$$

Recalling that

$$\varepsilon_{2s} = \varepsilon_{2c} = \varepsilon_2^*$$

and solving for ν^*,

$$\nu^* = \frac{E^* A^*}{\frac{E_s A_s}{\nu_s} + \frac{E_c A_c}{\nu_c}} \tag{14}$$

Now all of the quantities on the right side of Equation (14) are known and ν^* for this analysis using measured values becomes 0.3240.

C. REINFORCEMENT EFFECT FOR INTERIOR REGIONS

One of the intermediate steps in determining the actual specimen strain at the interior points away from the free boundary is to develop a correction factor for the full reinforcement of the specimen. By referring to Figure 4, it follows that P_c does not equal zero but is actually equal to the shear in the interface between the coating and the specimen, which is the mechanism by which the load is transferred to the coating. As shown in Figure 5, Zandman et al [Ref. 7] have determined that the full reinforcement takes place approximately four coating thicknesses in from a free boundary. For this analysis, full reinforcement was assumed at the first measured interior point. The first interior point was at 0.125 inches in from the boundary. Using the measured coating thickness divided into 0.125 equals 3.27. This point on Figure 5 yields less than a 5% correction factor.

Zandman, et al [Ref. 7] made the following development for reinforcement effects. Recalling that

$$P = P_s + P_c$$

where

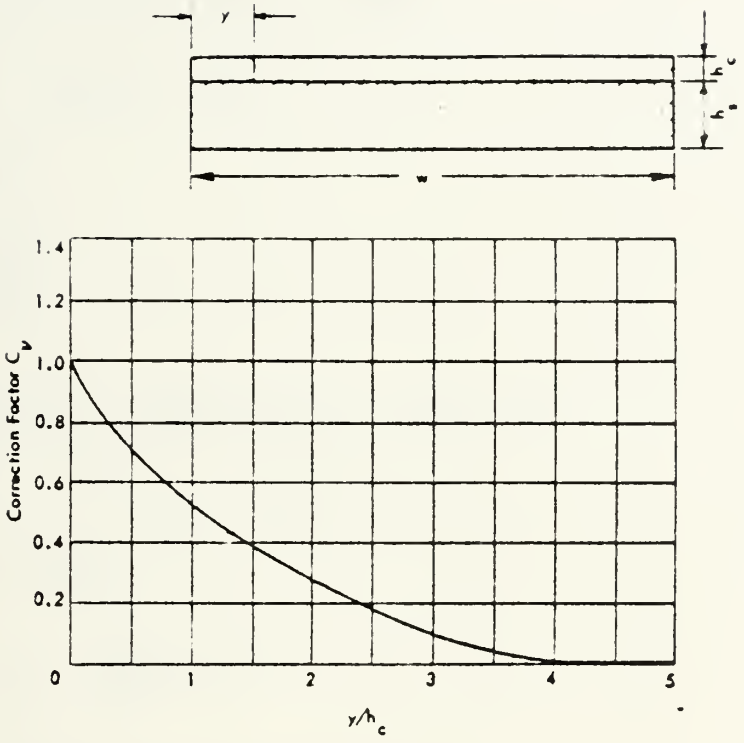

CORRECTION FACTOR C AS A FUNCTION OF POSITION y/h_c ACROSS THE TRANSITION ZONE [Ref. 7]

Figure 5

$$P = \sigma_{1u} A_s$$

$$P_s = \sigma_{1s} A_s \qquad (15)$$

$$P_c = \sigma_{1c} A_c$$

where σ_{1u} = Stress in the uncoated specimen.

It follows from Equation (2) that

$$\sigma_{1u}A_s = \sigma_{1s}A_s + \sigma_{1c}Ac \cdot \qquad (16)$$

From Figure 5,

$$A_s = h_s dy$$

$$A_c = h_c dy \qquad (17)$$

and therefore by substitution into (16)

$$h_s dy\sigma_{1u} = h_s dy\sigma_{1s} + h_c dy\sigma_{1c} \qquad (18)$$

Rearranging terms,

$$\sigma_{1u} = \sigma_{1s} + \frac{h_c}{h_s} \sigma_{1c} \qquad (19)$$

and by a similar development,

$$\sigma_{2u} = \sigma_{2s} + \frac{h_c}{h_s} \sigma_{2c} \cdot \qquad (20)$$

Recalling that

$$\varepsilon_{1c} = \varepsilon_{1s}, \ \varepsilon_{2c} = \varepsilon_{2s}$$

and using the plane stress equations

$$\sigma_1 = \frac{E}{1-\nu^2} (\varepsilon_1 + \nu\varepsilon_2) \qquad (21)$$

and

$$\sigma_2 = \frac{E}{1-\nu^2} (\varepsilon_2 + \nu\varepsilon_1), \tag{22}$$

substitution into Equations (19) and (20) and subtracting the results yields

$$\frac{E_s}{1-\nu_s^2} (\varepsilon_{1u} - \varepsilon_{2u}) (1 - \nu_s) =$$

$$\frac{E_s}{1-\nu_s^2} (\varepsilon_{1s} - \varepsilon_{2s}) (1 - \nu_s) + \tag{23}$$

$$\frac{h_c}{h_s} \frac{E_c}{1-\nu_c^2} (\varepsilon_{1c} - \varepsilon_{2c}) (1 - \nu_c) .$$

Rearranging terms and letting

$$\varepsilon_{1s} - \varepsilon_{2s} = \varepsilon_{1c} - \varepsilon_{2c}$$

it follows that

$$\varepsilon_{1u} - \varepsilon_{2u} = [1 + \frac{E_c}{E_s} \frac{h_c}{h_s} \frac{(1 + \nu_s)}{(1 + \nu_c)}] (\varepsilon_{1c} - \varepsilon_{2c}) . \tag{24}$$

The quantities in the brackets are all known and Equation (24) becomes

$$\varepsilon_{1u} - \varepsilon_{2u} = 1.0051 (\varepsilon_{1c} - \varepsilon_{2c}) . \tag{25}$$

This basically says that the photoelastic results of the interior points must be multiplied by 1.0051 to obtain the true results for an unreinforced specimen.

D. POISSON'S RATIO MISMATCH NEAR THE EDGE

Now that the interior reinforced regions have been corrected, it is appropriate to resolve the Poisson's ratio mismatch from the free boundary to approximately four thicknesses in. First by subtracting Equation (20) from (19), the relation

$$\sigma_{1u} - \sigma_{2u} = (\sigma_{1s} - \sigma_{2s}) + \frac{h_c}{h_s} (\sigma_{1c} - \sigma_{2c}) \tag{26}$$

results. By using the plane stress equations, it follows that

$$\begin{aligned} \sigma_{1s} - \sigma_{2s} &= \frac{E_s}{(1 - \nu_s^2)} [(\varepsilon_{1s} - \varepsilon_{2s}) + \nu_s (\varepsilon_{2s} - \varepsilon_{1s})] \\ &= \frac{E_s}{(1 + \nu_s)} [\varepsilon_{1s} - \varepsilon_{2s}] \\ &= \frac{E_s}{(1 + \nu_s)} [\varepsilon_{1c} - \varepsilon_{2c}] . \end{aligned} \tag{27}$$

As implied above, near the boundary ν_c is not homogeneous. Let $\nu_c = \bar{\nu}(x)$. In the coating

$$\sigma_{1c} = \frac{E_c}{(1 - \bar{\nu}^2} [\varepsilon_{1c} - \bar{\nu}\varepsilon_{2c}] \tag{28}$$

and

$$\sigma_{2c} = \frac{E_c}{1 - \bar{\nu}^2} [\varepsilon_{2c} + \bar{\nu}\varepsilon_{1c}] . \tag{29}$$

By subtracting and cancelling as above

$$\sigma_{1c} - \sigma_{2c} = \frac{E_c}{1 + \bar{\nu}} \left[\varepsilon_{1c} - \varepsilon_{2c}\right] . \qquad (30)$$

Substituting Equation (30) into (26)

$$\sigma_{1u} - \sigma_{2u} = \left[\frac{E_s}{1 + \nu_s} + \frac{E_c}{1 + \bar{\nu}}\right] (\varepsilon_{1c} - \varepsilon_{2c}) . \qquad (31)$$

Since

$$\varepsilon_{1c} - \varepsilon_{2c} = F_\varepsilon \, N$$

and

$$F_\varepsilon = \left(\frac{1 + \bar{\nu}}{E_c}\right) F_\sigma ,$$

it follows that

$$\sigma_{1u} - \sigma_{2u} = \left[\frac{E_s}{E_c} \frac{1 + \bar{\nu}}{1 + \nu_s} + \frac{h_c}{h_s}\right] F_\sigma \, N . \qquad (32)$$

By using the graph from Figure 5 and letting the variable on the curve be C(x),

$$\bar{\nu} = \nu^* + C(x) \, (\nu_c - \nu^*) . \qquad (33)$$

Equation (33) will give the Poisson's ratio, $\bar{\nu}$, needed to find the solution to Equation (32) since all other quantities will be known. For C(x) = 1 at the free boundary and for previously determined values of ν^* and ν_c, it follows that $\bar{\nu} = \nu_c$. For the first interior point at 0.125 inches, C(x) = 0 and $\bar{\nu} = \nu^*$.

V. DETERMINATION OF STRAINS USING OBLIQUE INCIDENCE MEASUREMENTS

The use of the oblique incidence adapter on the reflection polariscope provided the additional data necessary to calculate the longitudinal and transverse strains at given points away from the edge of the notch. Two types of data points are possible in this study since the first interior point away from the notch tip was assumed fully reinforced. A set of equations for the edge and a set for the interior regions were developed.

With the previous developments and those in Zandman, et al [Ref. 7], it is now possible to determine the working equations which will reduce fringe values to actual strain in a non-reinforced specimen. Beginning with Equations 2.24 [Ref. 6] and letting ν_c in those equations be $\bar{\nu}$.

$$\varepsilon_1 = \frac{f_\varepsilon}{2h_c} \frac{1}{(1+\bar{\nu})\sin^2\theta} [N_\theta(1-\bar{\nu})\cos\theta - N(\cos^2 - \bar{\nu})]$$

$$\varepsilon_2 = \frac{f_\varepsilon}{2h_c} \frac{1}{(1+\bar{\nu})\sin^2\theta} N_\theta(1-\bar{\nu})\cos\theta - N(1-\bar{\nu}\cos^2\theta) \tag{32}$$

where $F_\varepsilon = \frac{f_\varepsilon}{2h_c}$.

N_θ = Oblique incidence fringe reading

An equation can be derived which will reduce to the desired form where θ is 31° for the oblique incidence adapter used.

Using the results from the previous section for $\bar{\nu}$ at the edge, $\bar{\nu} = 0.2793$, the strains at the edge of the notch are given by

$$\varepsilon_1 = f_\varepsilon \, [1.4540N_\theta - .9712N]$$
$$\varepsilon_2 = f_\varepsilon \, [1.4540N_\theta - 1.9712N] \tag{33}$$

For the interior points where $\bar{\nu} = 0.3240$,

$$\varepsilon_1 = f_\varepsilon \, [1.6497N_\theta - 1.1692N]$$
$$\varepsilon_2 = f_\varepsilon \, [1.6497N_\theta - 2.1692N] \; . \tag{34}$$

These two equations now accurately describe the actual strain in the unbonded specimen using PS-1C Photoelastic Material bonded to 7075-T6 aluminum.

VI. EXPERIMENTAL COMPARISON OF STRESS CONCENTRATION IN A STRIP WEAKENED BY A CIRCULAR HOLE

To test the validity and accuracy of data taken utilizing the photoelastic method, a test case using a circular hole specimen of finite width was selected. R. C. J. Howland [Ref. 8] determined the stress distribution around the circular hole and with the known theoretical solution and the data points measured, it was possible to determine the accuracy of the photoelastic method.

A. EXPERIMENTAL PROCEDURE

A specimen was designed to accommodate a 2.0 inch diameter hole in the center. To determine a reasonable width and length which would allow a uniaxial field to exist between the center hole and the end grips, a 1/8 scale PS-1C model was tested under various tensile load conditions. It was determined that a minimum of a five-to-one ratio for length-to-width must exist to eliminate interference of fringe patterns. Figure 6 shows the full-scale 7075-T6 aluminum specimen and dimensions.

The aluminum specimen was placed under an 8000 pound load in the MTS machine, and both normal and oblique compensator readings were taken with a Model 032 Photolastic Compensator at 0.125 inch intervals at the 90° position on each side of the hole. Figure 7 shows the actual set-up

CIRCULAR HOLE SPECIMEN

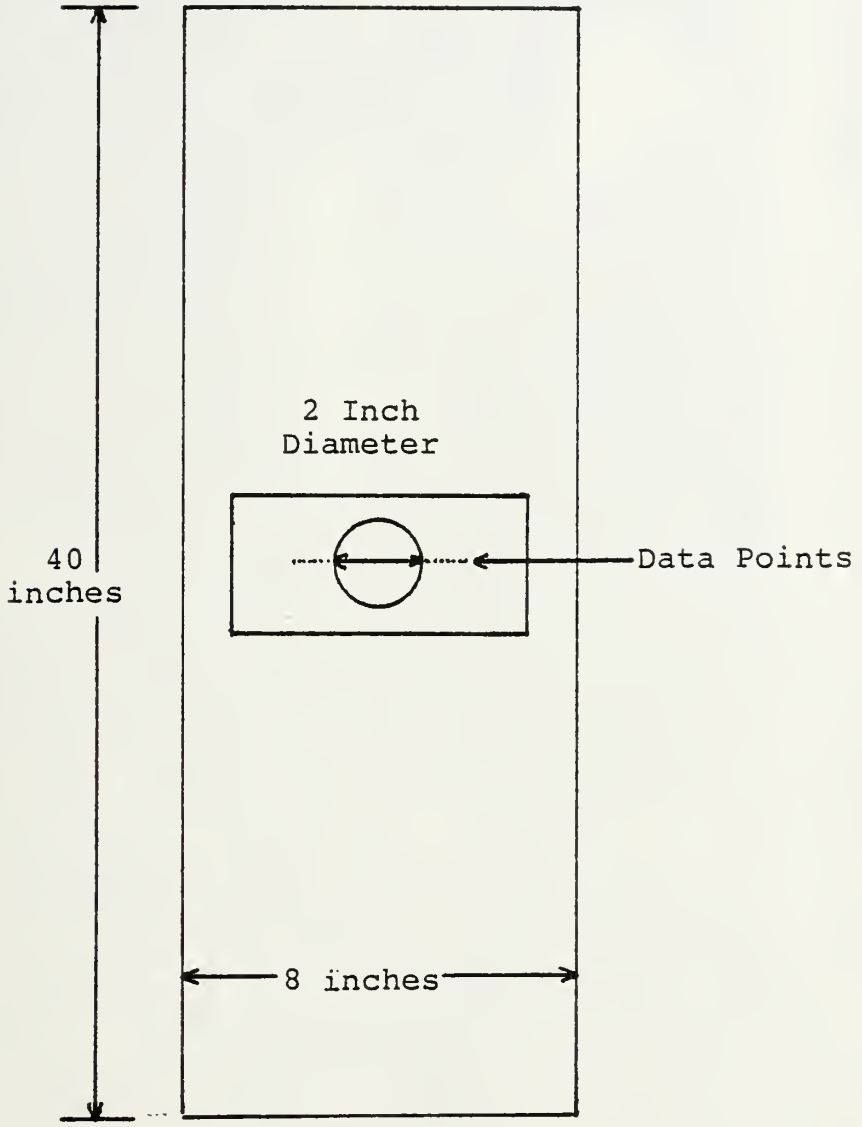

Figure 6

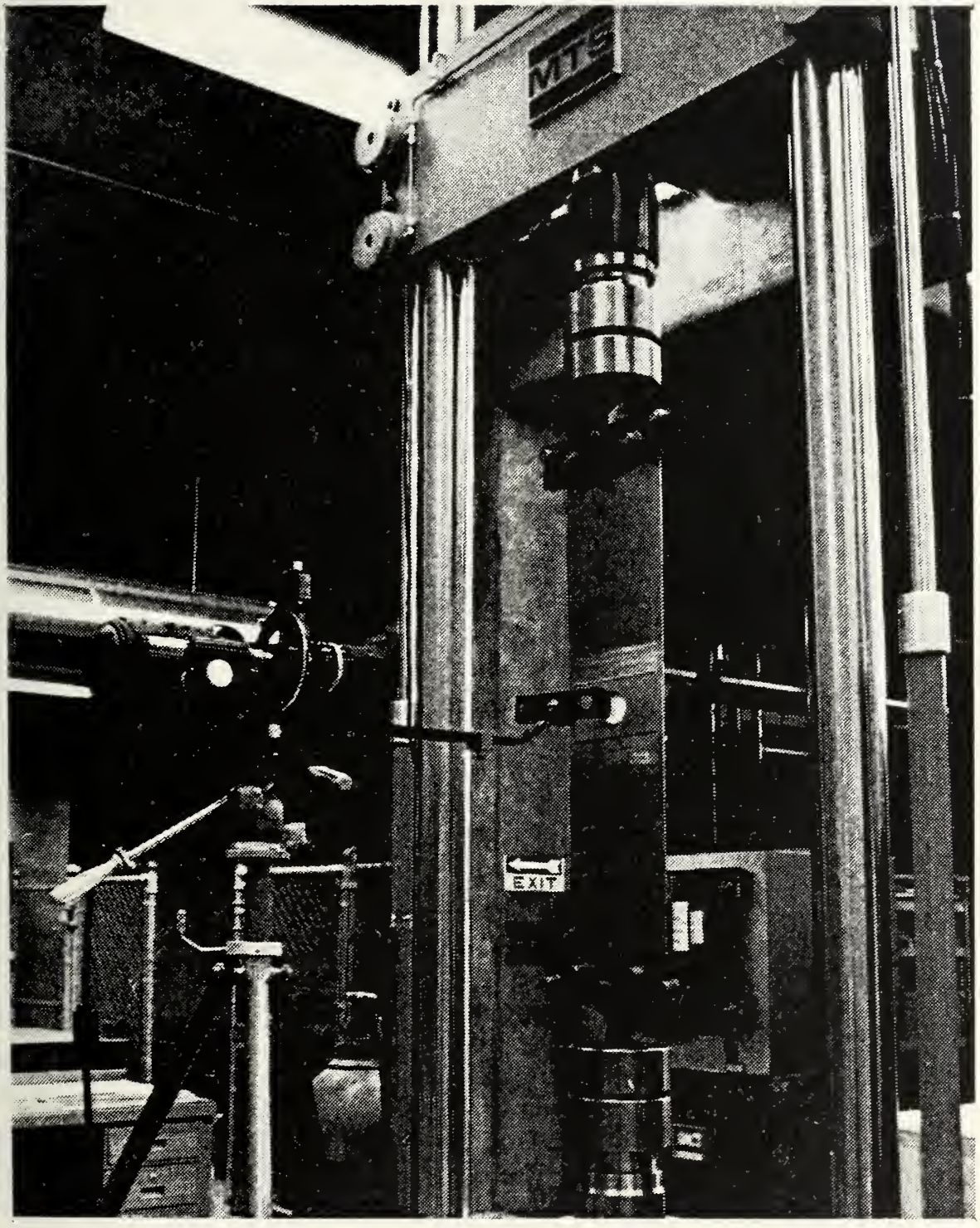

MTS MOUNTED CIRCULAR HOLE SPECIMEN

Figure 7

used. Figure 6 shows the data points, and Table V lists the compensator readings on both the left and right sides of the hole.

B. DATA COMPARISON

For the comparison to theory, the hole solution required was for $\lambda = 0.25$, where

$$\lambda = \frac{r}{b}$$

and

r = radius of the hole

b = half width of the strip.

Only the solutions for $\lambda = 0.2$ and $\lambda = 0.3$ were provided in Ref. 8; therefore, these two curves were plotted as shown in Figure 8, and the data points for $\lambda = 0.25$ were graphically determined by using the points on a curve midway between $\lambda = 0.2$ and $\lambda = 0.3$. Using the resulting K_T values and knowing that Howland [Ref. 8] used the far-field cross-sectional area of the specimen to determine K_T, the comparisons in Table VI were generated. From the comparison, a range of 0.2% to 1.4% difference resulted.

C. PHOTOELASTIC METHOD ACCURACY

In the references used for this thesis, the general concensus is that photoelastic methods are accurate to within 5.0%. The accuracy attained in this comparison was much better, even with the graphical interpolation of the $\lambda = 0.25$

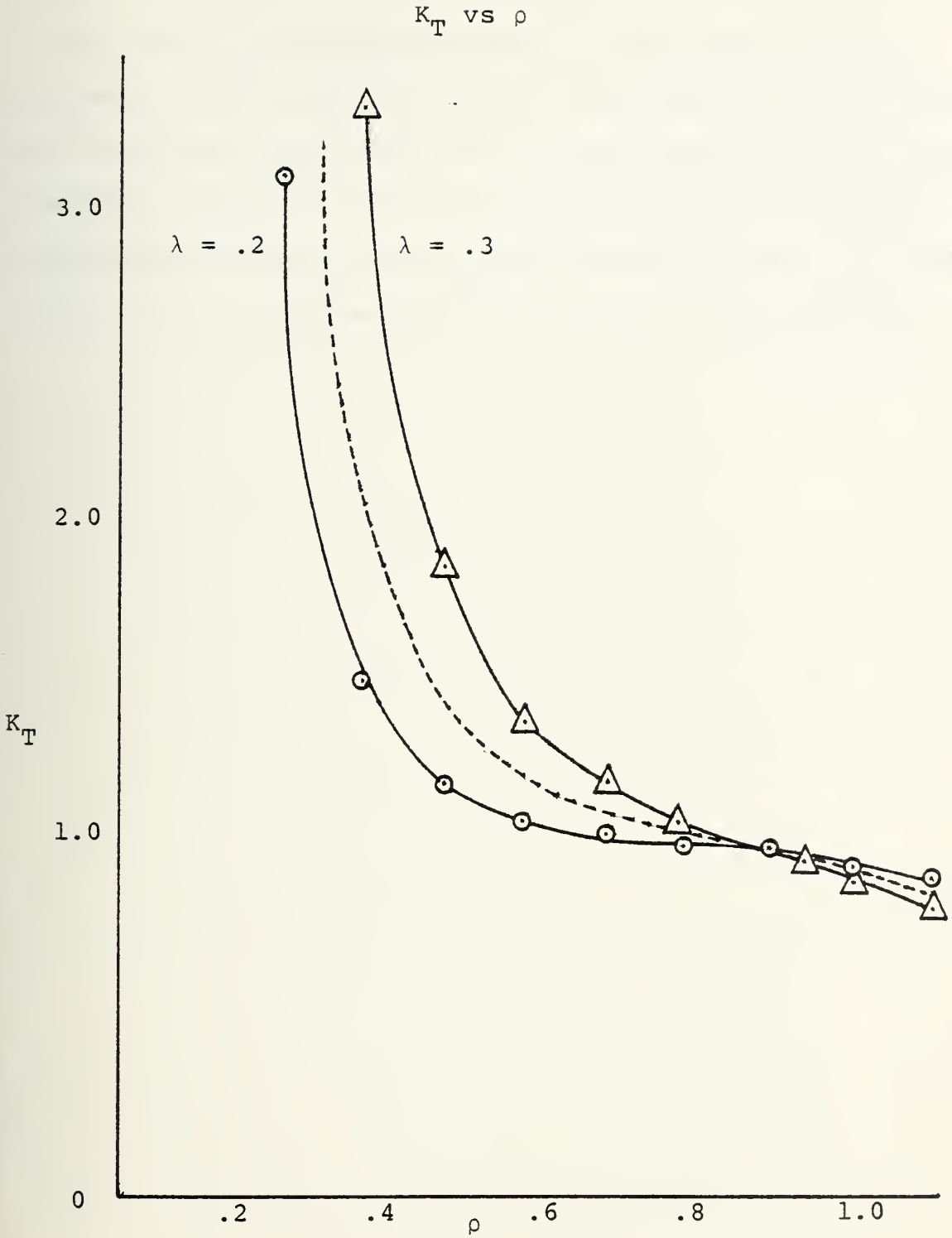

Figure 8

curve. The explanation offered for this close correlation is the use of the telemicroscope in conjunction with a procedure wherein each data point was measured three times, and the value itself was taken as the average of the three readings. Also, the careful measurement of all material properties improved the accuracy several percent over that which could be obtained with published, nominal values.

VII. UNBOND CHARACTERISTICS OF A NOTCHED SPECIMEN

During specimen preparation, it is possible to inadvertently introduce a weak bond area between a specimen and the photoelastic material, which would cause a change in the fringe number in that weak area. This study was undertaken to determine the amount of bond failure required to show significant change in fringe values.

A. EXPERIMENTAL PROCEDURE

As indicated in Figure 9, an aluminum specimen with PS-1C Photoelastic Material bonded to it was prepared with intentionally created unbond areas of known size between the PS-1C and the aluminum. The 0.5 inch diameter paper discs with adhesive backing were applied at the points indicated in Figure 9. Enough oil to cover each disc with a thin film was applied prior to bonding material application. Preparation and photoelastic material application were done according to instructions provided by Photoelastic Inc. After proper drying time, the specimen was loaded in 1000 pound increments up to 15,000 pounds in the MTS machine, and compensator readings were taken in the normal direction. This selection of points allowed for both elastic and plastic region investigation. A second specimen was prepared with no known unbonds or weak areas and loaded according to the same schedule as a control specimen.

UNBOND SPECIMEN

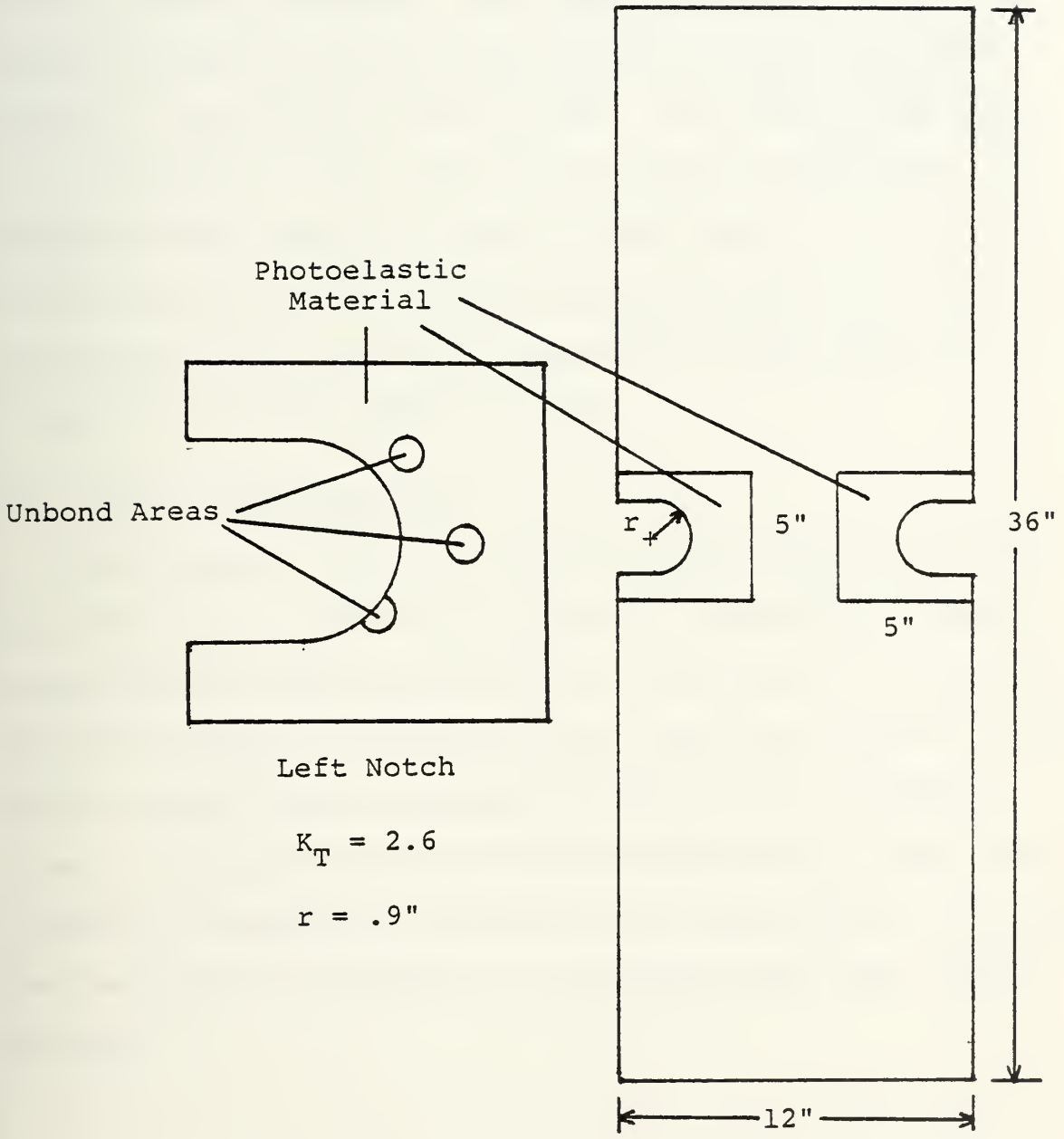

Figure 9

B. UNBOND TEST RESULTS

Figure 10 clearly shows a problem with the unbond specimen. Close visual examination of photos taken of each specimen at similar loads showed a clearer, more uniform pattern in the control specimen. The unbond specimen showed rough, fuzzy fringes with barely discernable changes in pattern shape at the interior unbond areas. The area at the notch tip displayed the most significant pattern difference. As indicated by Figure 10, above the 5000 pound load, or in a 5320.0 psi stress level in the principle direction, this particular unbond specimen dropped off at the rate of 0.2 fringes for 10,000 pounds of load.

C. UNBOND CHARACTERISTICS

Weak bonds of the type studied are difficult to detect, but they can be seen if the operator is familar with the rough pattern characteristics of the weak bond. The problem with the unbond is confined to the immediate vicinity of the weak area and does not appear to effect the surrounding areas. Weak bond areas can be tolerated only if they are located at distances sufficiently far from points of interest so that they do not distort or interfere with local fringe patterns.

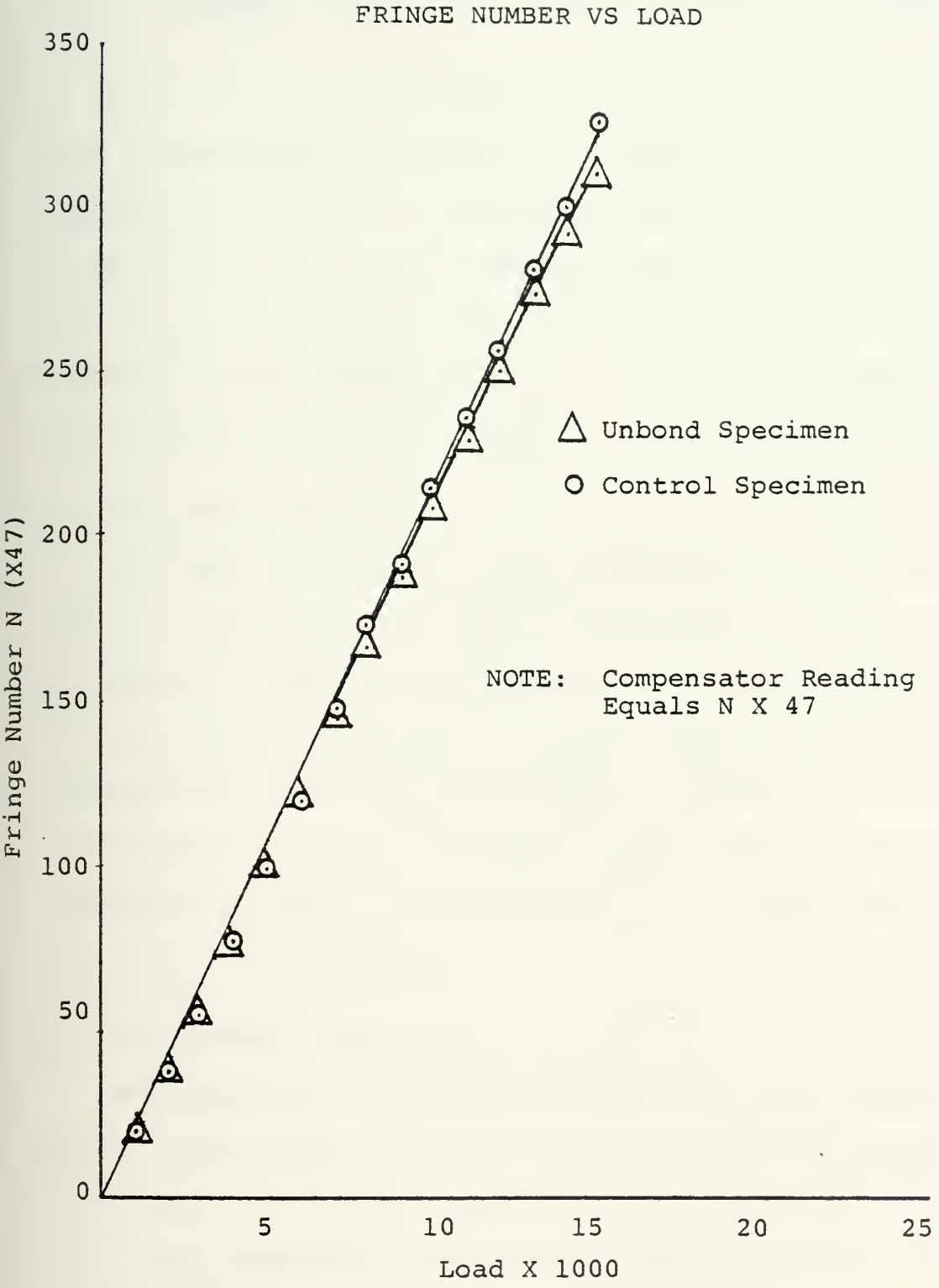
FRINGE NUMBER VS LOAD
350
300
250
200
150
100
50
0
Fringe Number N (X47)
Unbond Specimen
Control Specimen
NOTE: Compensator Reading
Equals N X 47
5
10
15
20
25
Load X 1000

Figure 10

VIII. LINEARLY ELASTIC ZONE INVESTIGATION OF A NOTCHED SPECIMEN

Several proposals in the area of fracture theory analysis have indicated that in addition to stress concentration factors, information on the stress distribution at a notch is required. This study provides carefully measured longitudinal and transverse stress distributions of that area obtained by the photoelastic method. Oversized specimens were used to increase the accuracy of photoelastic results.

A. SPECIMEN PREPARATION

The basic dimensions of the specimens used by Stuart [Ref. 9] and Engle [Ref. 10] were doubled in size as shown in Figure 11. The stress concentration factors of 3.8 and 2.6 were retained in order to compare data points. Each specimen was bonded with photoelastic material from the same lot number and nominal thickness as that used in the characterization to retain the accuracy of correction factors and data reduction techniques.

B. EXPERIMENTAL PROCEDURE

Each specimen was loaded in tension in the linearly elastic zone using the Tinius-Olsen set-up shown in Figure 12. Normal and oblique compensator readings were taken at 0.125 inch intervals from the notch tip for loads of 15,000

LARGE SPECIMEN GEOMETRIES

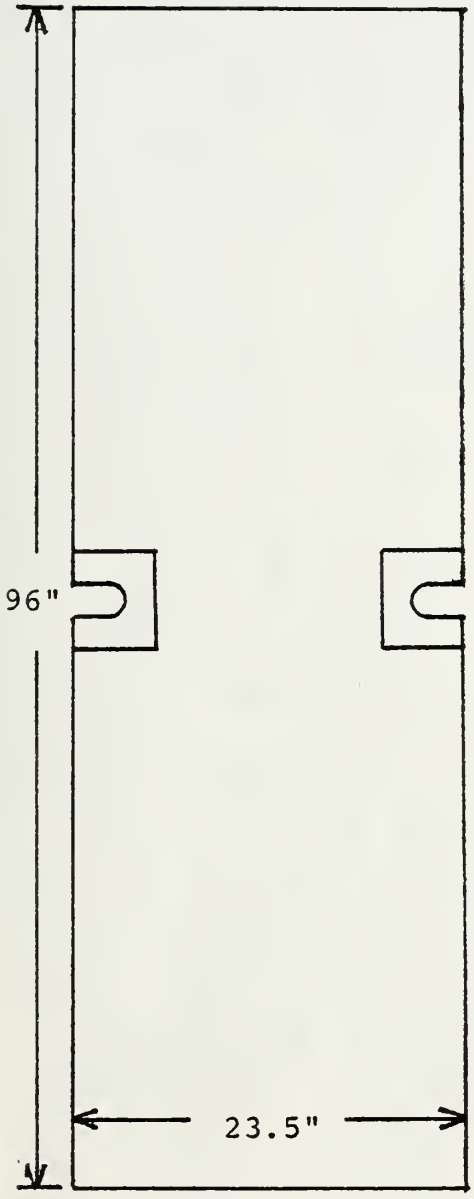

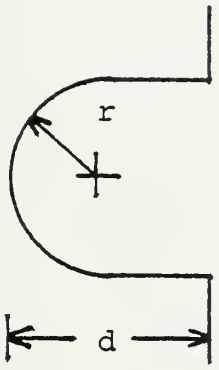

Nominal K_T	2.6	3.8
r(in)	1.8125	0.625
d(in)	2.875	3.938
Reduced Cross-section (in^2)	17.75	15.63

7075-T6 Aluminum
Thickness 0.080 in

Figure 11

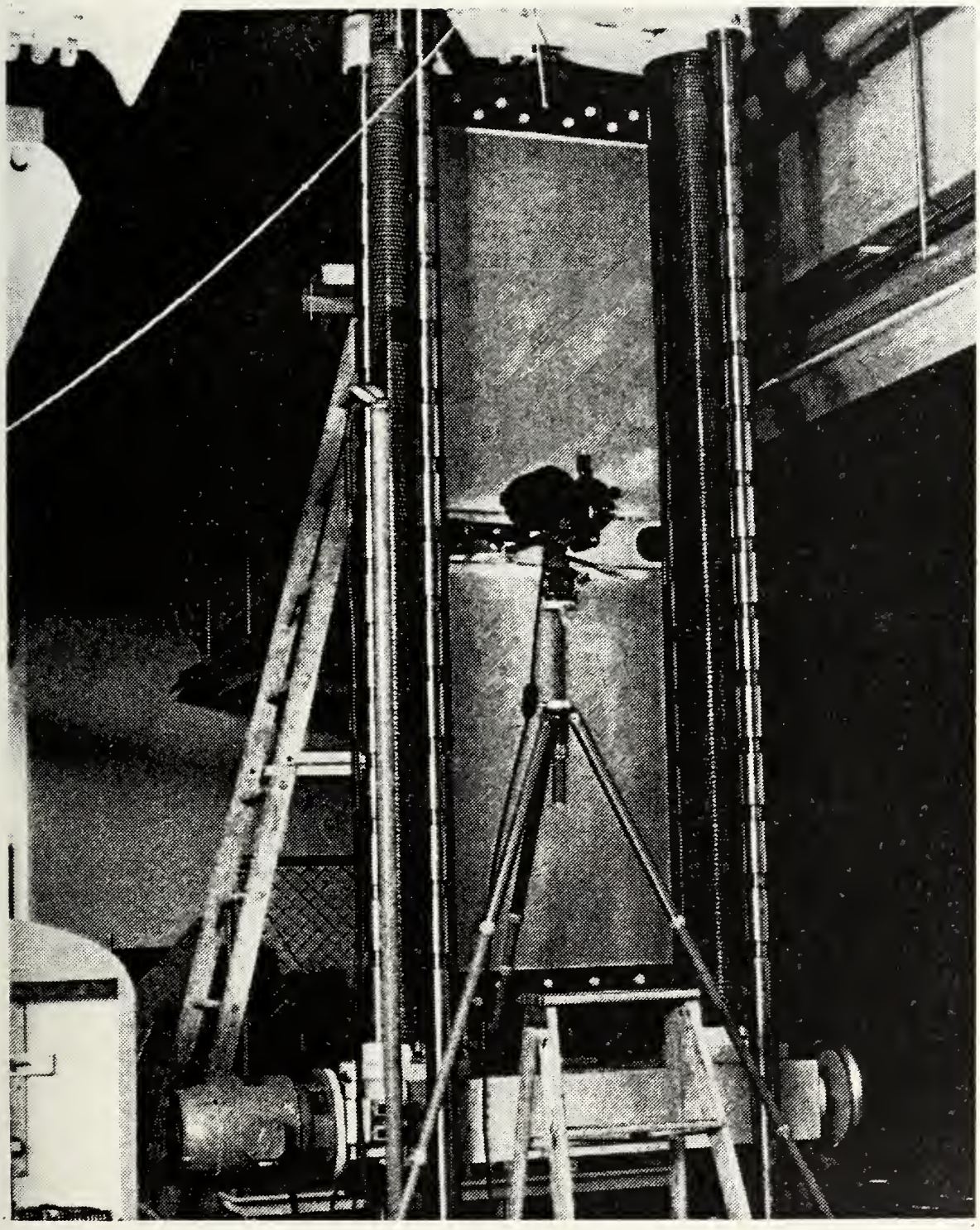

LARGE SPECIMEN MOUNTED IN THE TINIUS-OLSEN

Figure 12

and 20,000 pounds for the K_T = 3.8 notch and loads of 10,000, 15,000 and 20,000 pounds for the K_T = 2.6 notch. The results of the K_T = 3.8 notch loads are tabulated in Tables VIII and IX while the K_T = 2.6 notch results are shown in Tables XIII, XIV, and XV. Figures 13 and 14 depict the stress distributions at positions on the line of symmetry extending outward from the notch tip for both the longitudinal and transverse directions. Normalized curves are also indicated in Figures 13 and 14.

C. ELASTIC ZONE CHARACTERISTICS

The use of large specimens provided a much more detailed view of the notch tip region and allowed for an accurate assessment of the stress gradient near the notch tip in the elastic zone. No other data was available to compare measurements with theory, but the characteristic shape of the stress curve compares favorably with that of Kim et al in Ref. 11. The normalized curve plots on Figures 13 and 14 demonstrate the proportionality and consistency of the measured data.

ELASTIC REGION
K_T = 3.8
STRESS vs DISTANCE

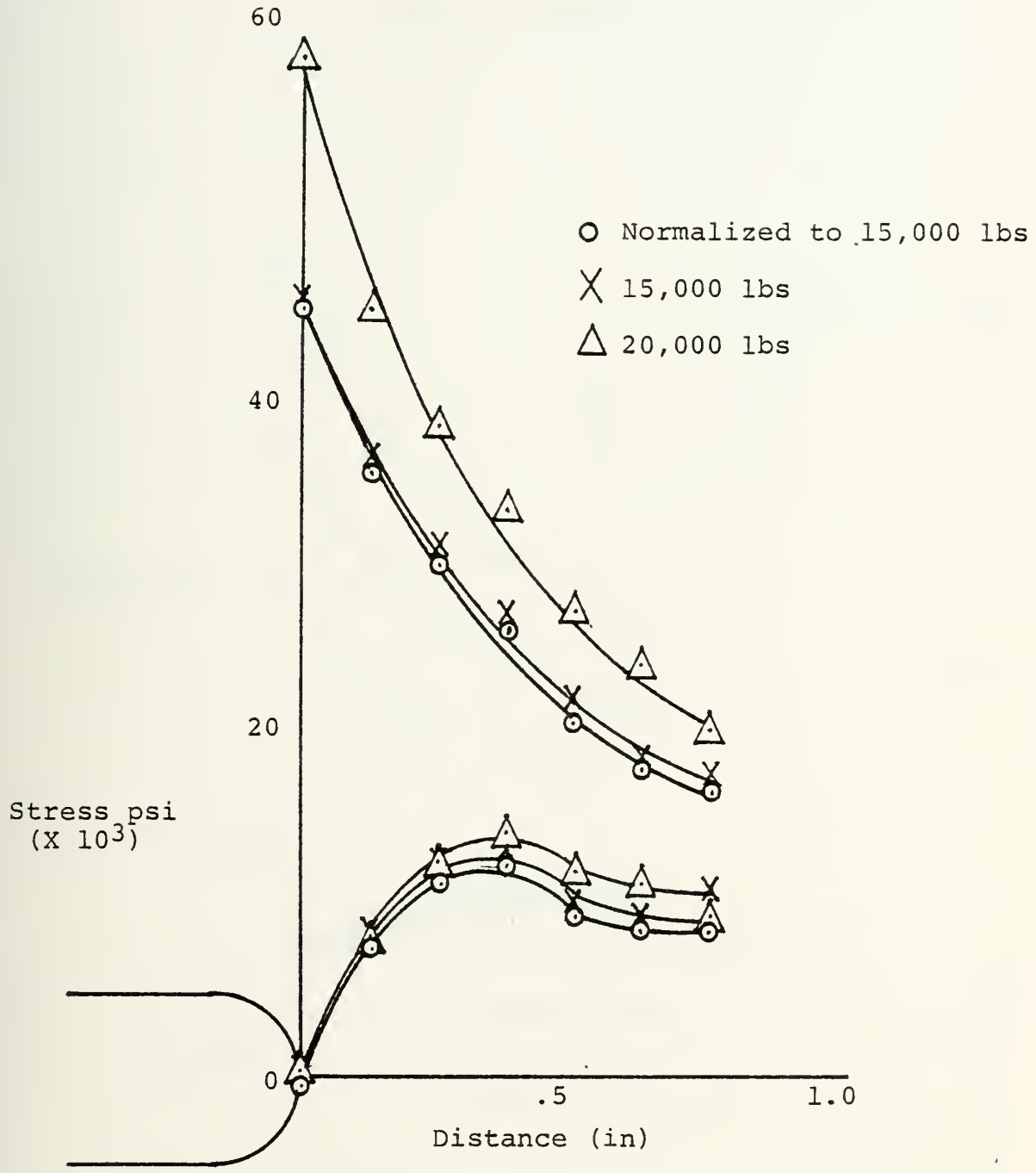

Figure 13

ELASTIC REGION
K_T = 2.6
Stress vs Distance

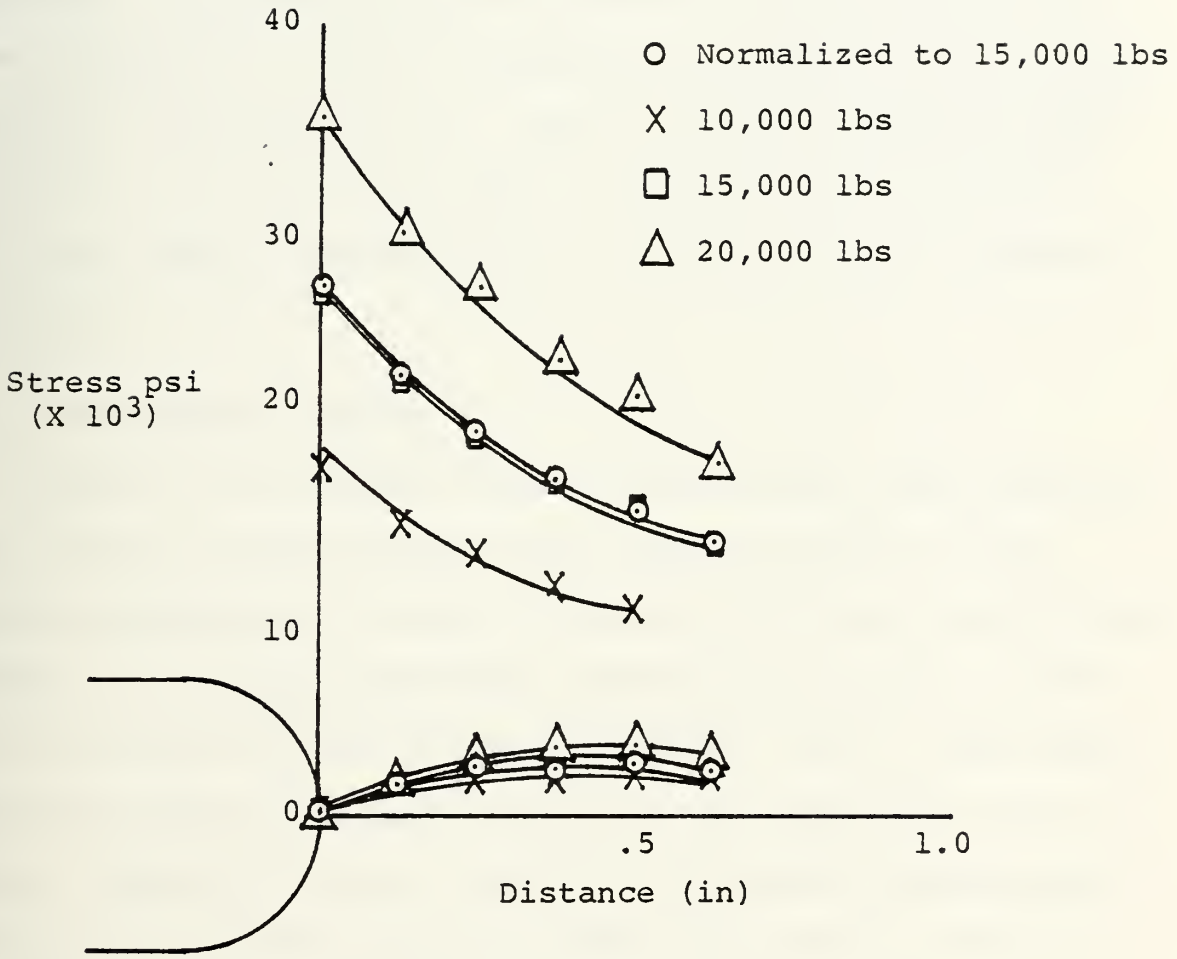

Figure 14

IX. EXPERIMENTAL DETERMINATION OF THE PLASTIC ZONE AND RESIDUAL COMPRESSIVE STRESS

If a notched specimen is subjected to a large tensile load below the yield point of the material in the far-field regions, it is possible to cause the area in the vicinity of a notch to yield and create a plastic zone. When the specimen is unloaded, the surrounding unyielded portion of the specimen will cause a residual compressive stress to be produced around the notch. Using a modified Ramberg-Osgood approach, an attempt was made to characterize the plastic zone and compare the results to slip-line theory and Neuber's relation.

A. EXPERIMENTAL PROCEDURE

The K_T = 2.6 specimen used for the elastic zone analysis was loaded to strain levels well into the plastic region which coincided with loads of 60,000, 65,000 and 70,000 pounds. Normal and oblique compensator readings were taken at each load level and at the no load condition. The no load condition was measured as each load level was taken back down to zero. Tables XVI, XVII, and XVIII contain the measured and reduced data, while Figure 16 shows the graphical results for the plastic region. The residual compressive stresses were plotted in Figure 21.

The K_T = 3.8 specimen was lost on the first load into the plastic region due to a bond failure. For the K_T = 2.6 specimen, a higher elongation percentage bonding agent was chosen, PC-8, which allowed more flexibility in choosing strain levels. Tables X and XI were retained to provide data for the K_T = 3.8 notch beyond the elastic region and into the early plastic region prior to bond separation.

B. DATA REDUCTION METHOD

In order to reduce fringe values to stresses, it becomes necessary to develop a method of data reduction which fits both the elastic and the plastic regions. The previous photoelastic development, derived to handle the purely elastic region which uses the linear stress-strain law, has been applied to the data in that range. To reduce the fringe numbers in the plastic range to stresses, the data was first reduced to strain by the previous method. To obtain stresses, a nonlinear stress-strain law was used where it was assumed that the total strain was equal to the strain in the elastic region plus the strain in the plastic region.

$$\varepsilon = \varepsilon_e + \varepsilon_p \tag{35}$$

The total stress-strain expressions in the 1 and 2 directions, due to longitudinal and transverse loading, are derivable using linear superposition of the elastic strains. Referring to Figure 15a,

REPRESENTATIVE LOADING

Figure 15a

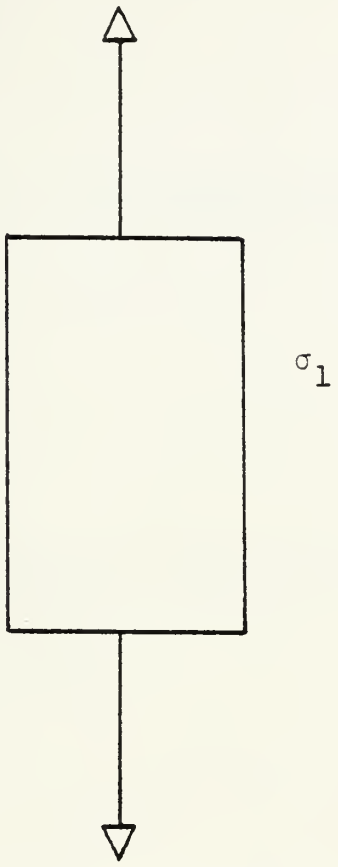

Figure 15b

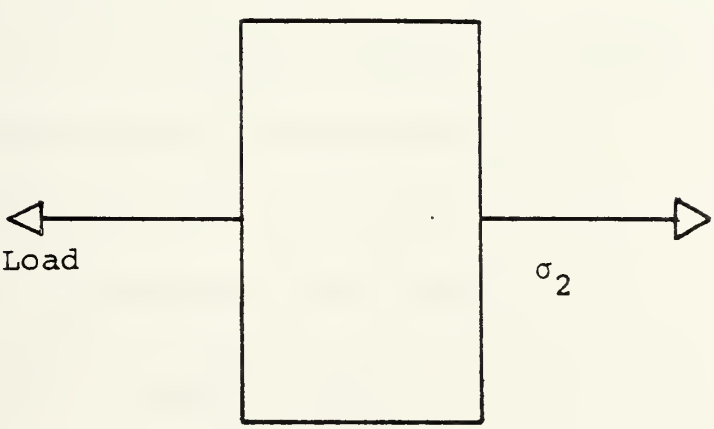

$$\varepsilon_1 = \frac{\sigma_1}{E}$$

and (36)

$$\varepsilon_2 = -\nu\varepsilon_1 = -\nu\frac{\sigma_1}{E}$$

for a longitudinal load. A transverse load from Figure 15b yields

$$\varepsilon_2 = \frac{\sigma_1}{E} \quad (37)$$

and

$$\varepsilon_1 = \nu\varepsilon_2 = -\nu\frac{\sigma_2}{E} .$$

Substitution back into Equation (35) now gives

$$\varepsilon_1 = \varepsilon_{p1} - \nu\varepsilon_{p2} + \frac{1}{E}[\sigma_1 - \nu\sigma_2] \quad (38)$$

and similarly

$$\varepsilon_2 = \varepsilon_{p2} - \nu\sigma_{p1} + \frac{1}{E}[\sigma_2 - \nu\sigma_1] \quad (39)$$

The strain in the plastic regions is handled using a modified Ramberg-Osgood method such that

$$\varepsilon_p = \beta\left(\frac{\sigma}{E}\right)^n \quad (40)$$

Substitution into Equation (39) yields

$$\varepsilon_1 = \beta\left(\frac{\sigma_1}{E}\right)^n - \nu\beta\left(\frac{\sigma_2}{E}\right)^n + \frac{1}{E}[\sigma_1 - \nu\sigma_2] \quad (41)$$

$$\varepsilon_2 = \beta\left(\frac{\sigma_2}{E}\right)^n - \nu\beta\left(\frac{\sigma_1}{E}\right)^n + \frac{1}{E}[\sigma_2 - \nu\sigma_1] \quad (42)$$

For this analysis $E = 10.11 \times 10^6$ psi which was measured by Engle [Ref. 10] on material from the same lot. It was

developed from strain gage data and had a 0.999994 correlation coefficient, and $\nu = 0.3238$ from the same strain data measured into the plastic region. Using a power curve fit on Garske's data [Ref. 2] measured on the same material in the plastic range resulted in $\beta = 3.8776 \times 10^{45}$ and $n = 22.678$.

To solve for the two unknown stresses in Equations (41) and (42) simultaneously, a nonlinear, simultaneous equation, FORTRAN program developed by K. M. Brown at Purdue was used. The program was listed in the Naval Postgraduate School computer's IMSL as a subroutine named NLNSYS.

The results of the computer analysis were tabulated in Tables XIX, XX, and XXI. Figures 16 and 17 depict the results of the stress and strain data reductions.

C. COMPARISON OF EXPERIMENTAL DATA WITH SLIP-LINE THEORY RESULTS

Classical slip-line theory for rigid, perfectly plastic materials as developed by Kachanov [Ref. 12] indicated that as the distance from the notch tip increases, the stresses at those points increase slightly as shown in Figure 18. As can be seen, the experimental data reduced by the modified Ramberg-Osgood method does not increase at any point beyond the tip value and as the distance from the tip increases, the two lines grow further apart. The transverse stress appears to have the same trend as the theory but also falls off.

PLASTIC REGION
K_T = 2.6

STRESS vs DISTANCE

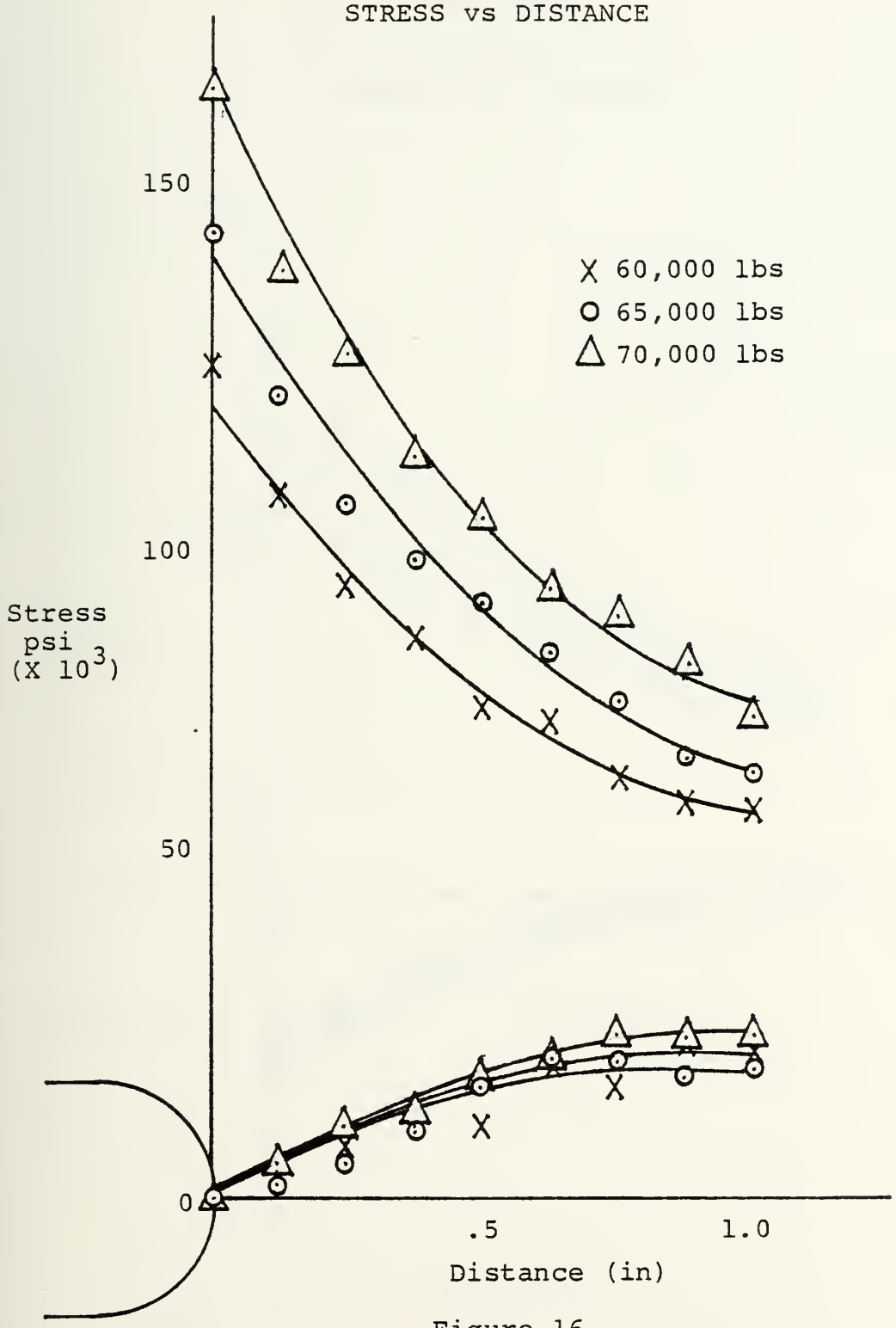

Figure 16

PLASTIC REGION

$K_T = 2.6$

STRAIN vs DISTANCE

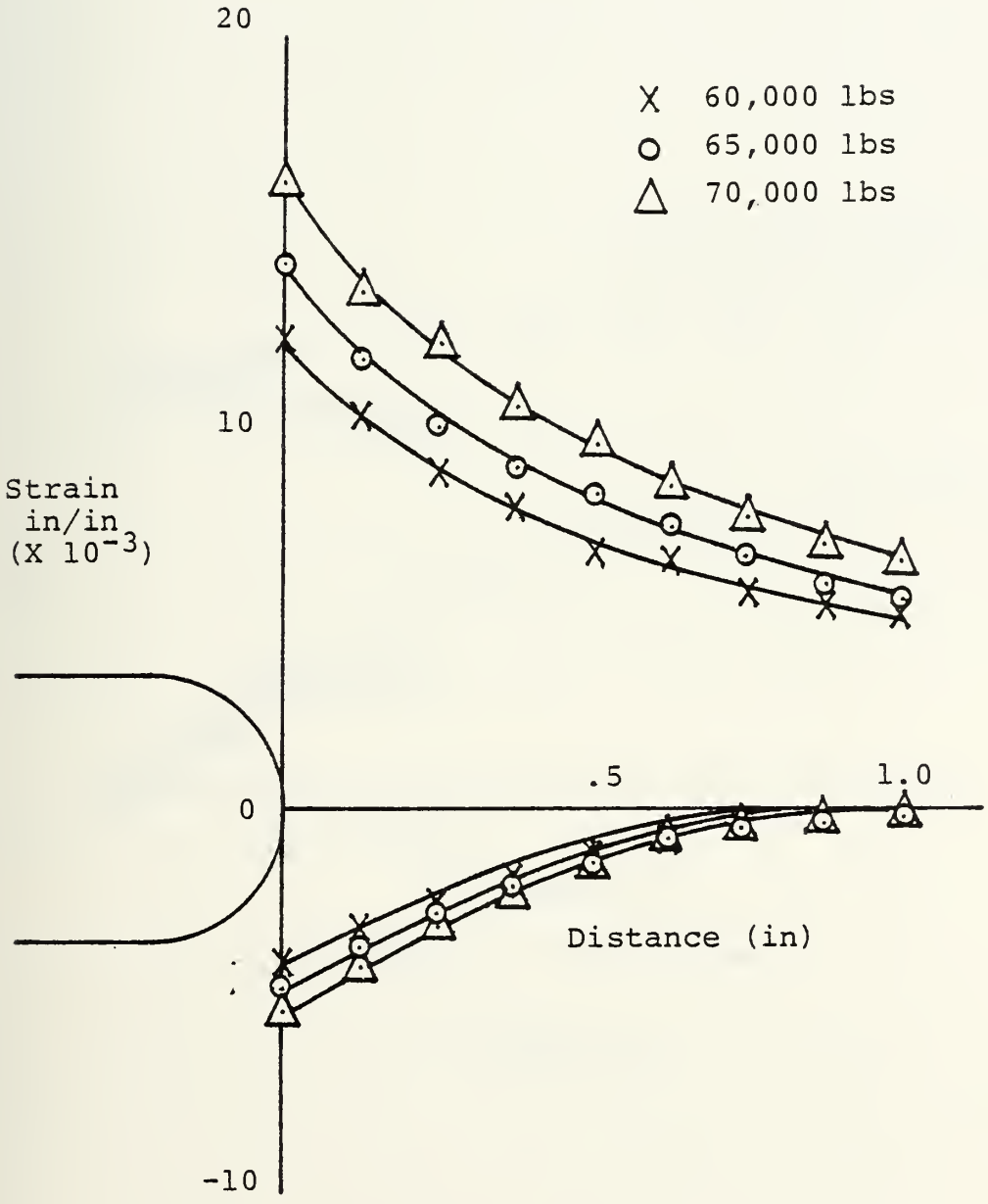

Figure 17

SLIP-LINE STRESSES COMPARED
TO EXPERIMENTAL STRESSES

K_T = 2.6, 70,000 lb Load

STRESS (NORMALIZED) vs DISTANCE

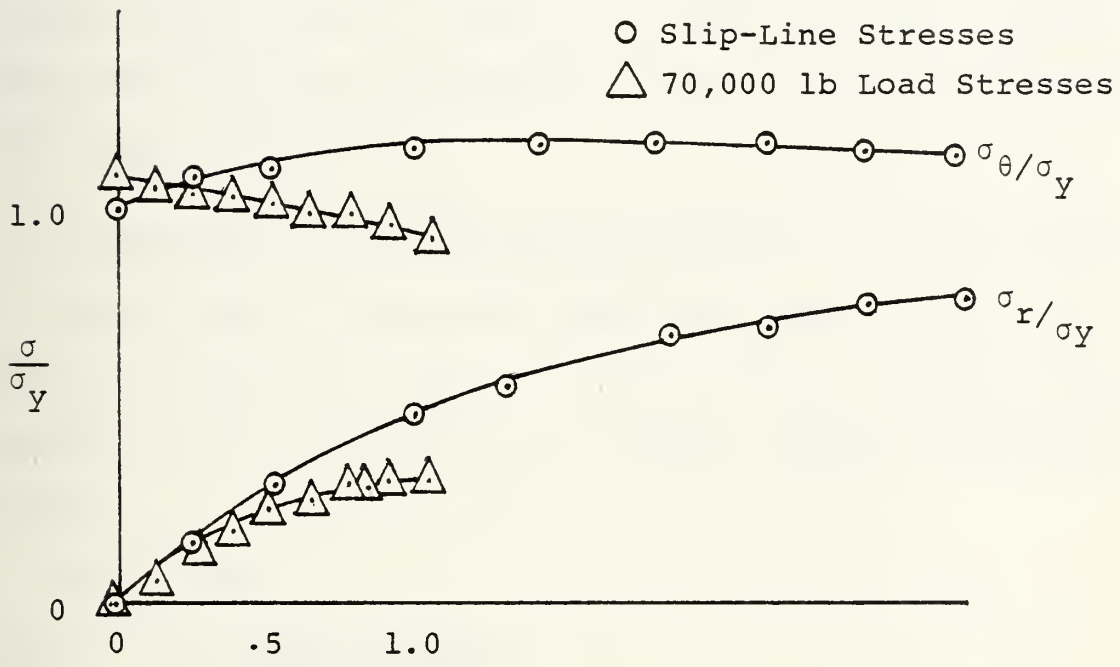

NOTE: σ_y = 74,500 psi

Figure 18

D. PLASTIC ZONE DETERMINATION

To further understand the actual regions depicted by each of the load points, the Von Mises Theory was applied as shown in Figure 19. To determine which of the points on the experimental curves were fully plastic, the yield stress level was plotted as indicated, and the results show that for the highest load, only the first three points were fully plastic. Referring back to Figure 18, the longitudinal stress still appears to contradict the approximate theory in this range, while the transverse stress follows the theoretical curve closely.

E. COMPARISON OF PLASTIC ZONE RESULTS WITH NEUBER'S RELATION

Neuber [Ref. 1] theorized that the geometric mean of a stress concentration factor, K_σ, and a strain concentration factor, K_ε, is equal to K_T, the elastic stress concentration factor

$$K_T^2 = K_\sigma K_\varepsilon$$

where $$K_\sigma = \frac{\text{local stress}}{\text{nominal stress}}$$

$$K_\varepsilon = \frac{\text{local strain}}{\text{nominal strain}}$$

This relation applies only at the edge of a hole; in this case at the notch tip. Table XXII clearly depicts the consistent inaccuracy of the above relation for this set of load levels and the $K_T = 2.6$ notch size. The design K_T value used in this study is calculated using the reduced

YIELD POINT PREDICTION

$\sigma_r^2 - \sigma_r\sigma_\theta + \sigma_\theta^2$ vs DISTANCE

X 60,000 lbs

O 65,000 lbs

△ 70,000 lbs

$\sigma_{eq} = \sigma_r^2 - \sigma_r\sigma_\theta + \sigma_\theta^2$

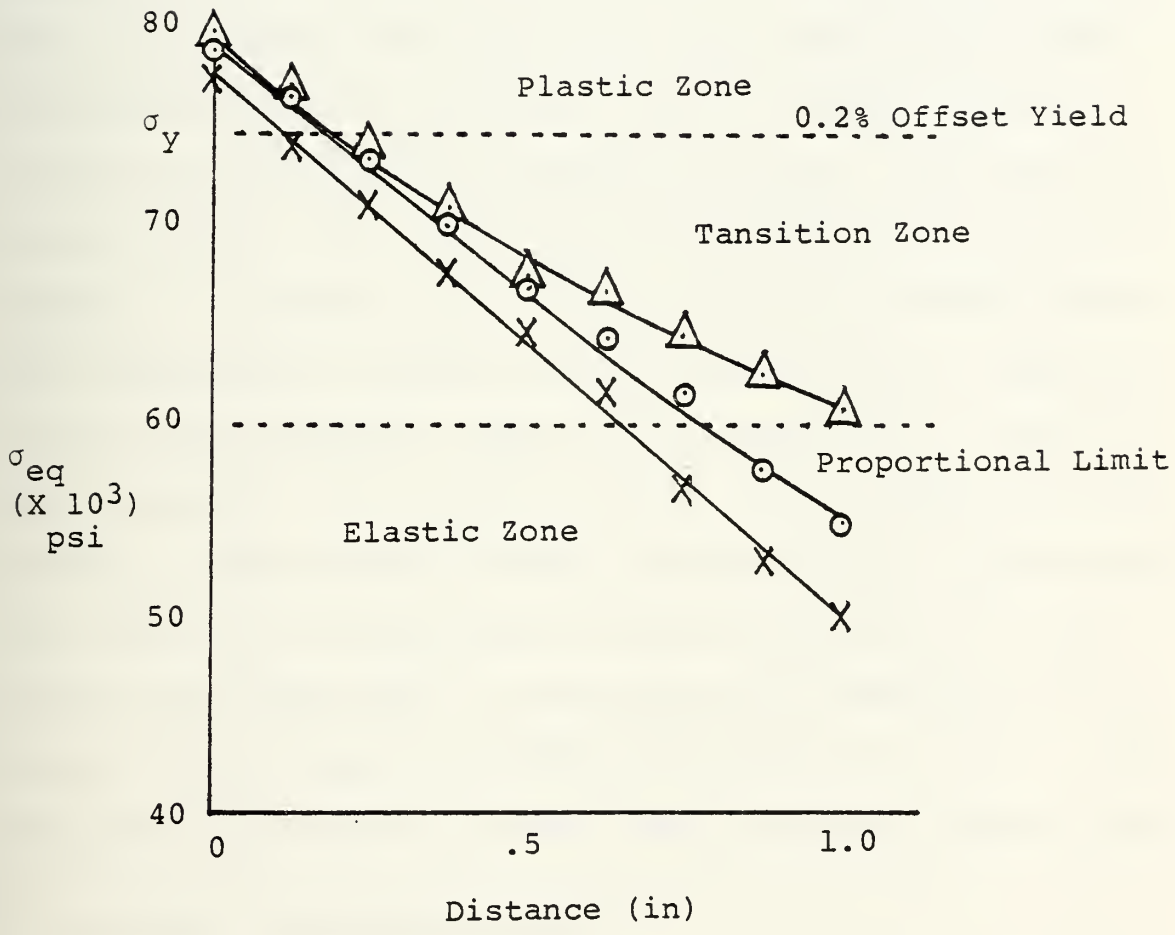

Figure 19

cross-section area while Neuber's K_T is based on the far-field area. For Neuber's K_T = 3.44, a spread of from 20.6% to 21.2% error resulted.

F. STRESS CURVE ANALYSIS FOR COMBINATION ELASTIC AND PLASTIC CURVES

If the classical stress-strain curve is recalled for 7075-T6 aluminum, it follows that a mapping of the stresses through a plastic zone into the elastic portion of the specimen, going outward from the notch tip, would display the characteristics of a nonlinear plastic stresses, then a transition from plastic to elastic stresses, and finally a linear elastic field. This is the essential explanation of Figure 20. Assuming that the data taken was accurate past the characteristic plastic zone around the notch, Figure 20 depicts an interesting result in the range of D = 0.65 in. when compared to pure elastic curves. It is seen that the material in that elastic region exhibits elastic characteristics, and it is interesting to note the similarity to the elastic curve and that on the continually changing curve a rather abrupt change to elastic-like behavior occurs. This study did not attempt to match those curvature similarities.

G. RESIDUAL COMPRESSIVE STRESS

After each loading into the plastic region, a complete unload was performed to obtain residual compression fringe values around the K_T = 2.6 notch. The resulting stresses

RAMBERG-OSGOOD PLASTIC REGION
SOLUTION COMPARED TO ELASTIC
REGION SOLUTION

STRESS vs DISTANCE

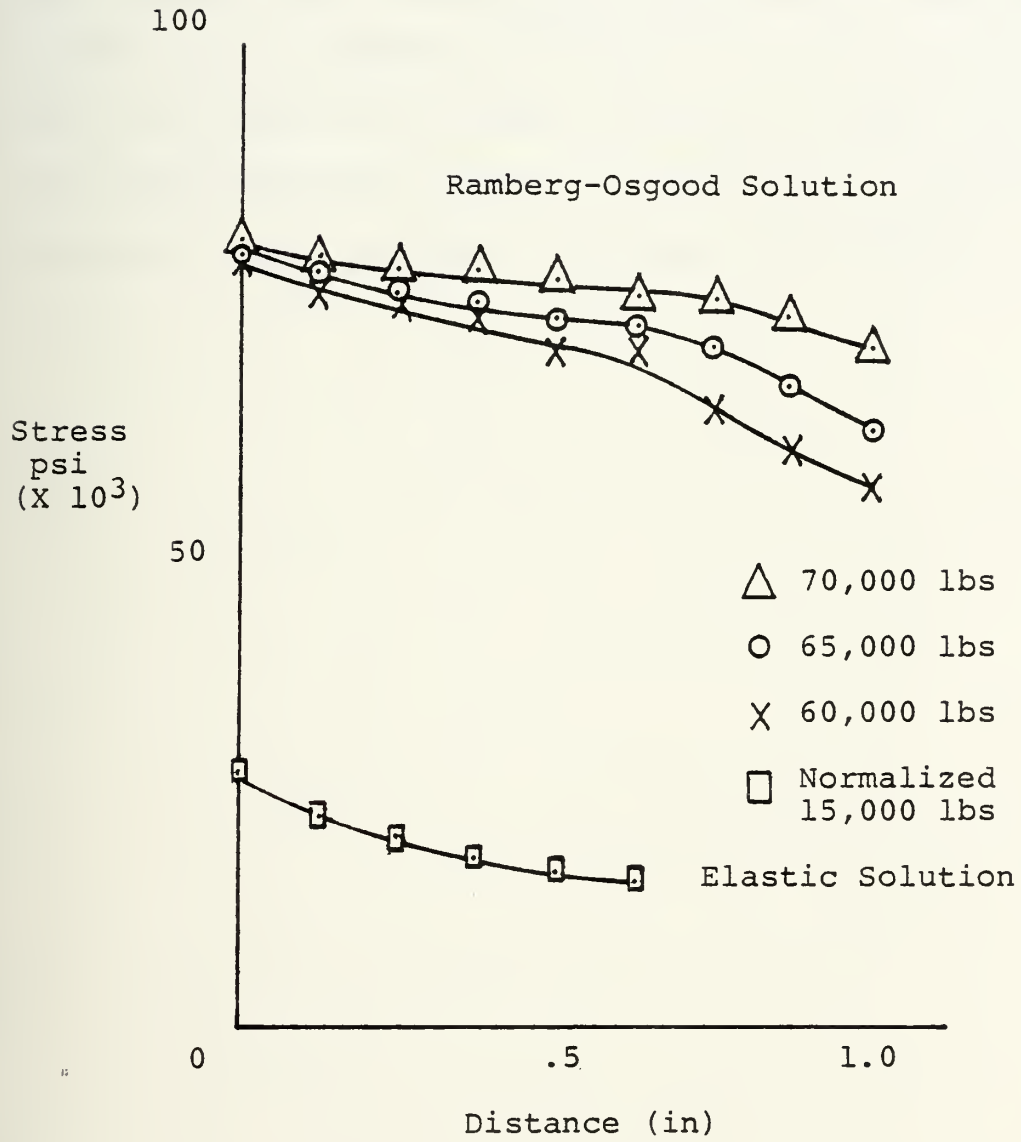

Figure 20

from Tables XVI, XVII, and SVIII were plotted against the distance from the notch tip in Figure 21. The stress levels in each case appear to converge on an unplotted point beyond D = 0.625 in where σ_1 and σ_2 are equal. Since the residual stresses were non-zero, this would indicate that yielding had occurred up to that point. Referring back to the regions indicated on Figure 19, it can be inferred that the plastic zone around the notch includes points in the transition zone. Washout of fringes at a possible convergent point precluded its exact determination.

RESIDUAL COMPRESSIVE STRESS

STRESS vs DISTANCE

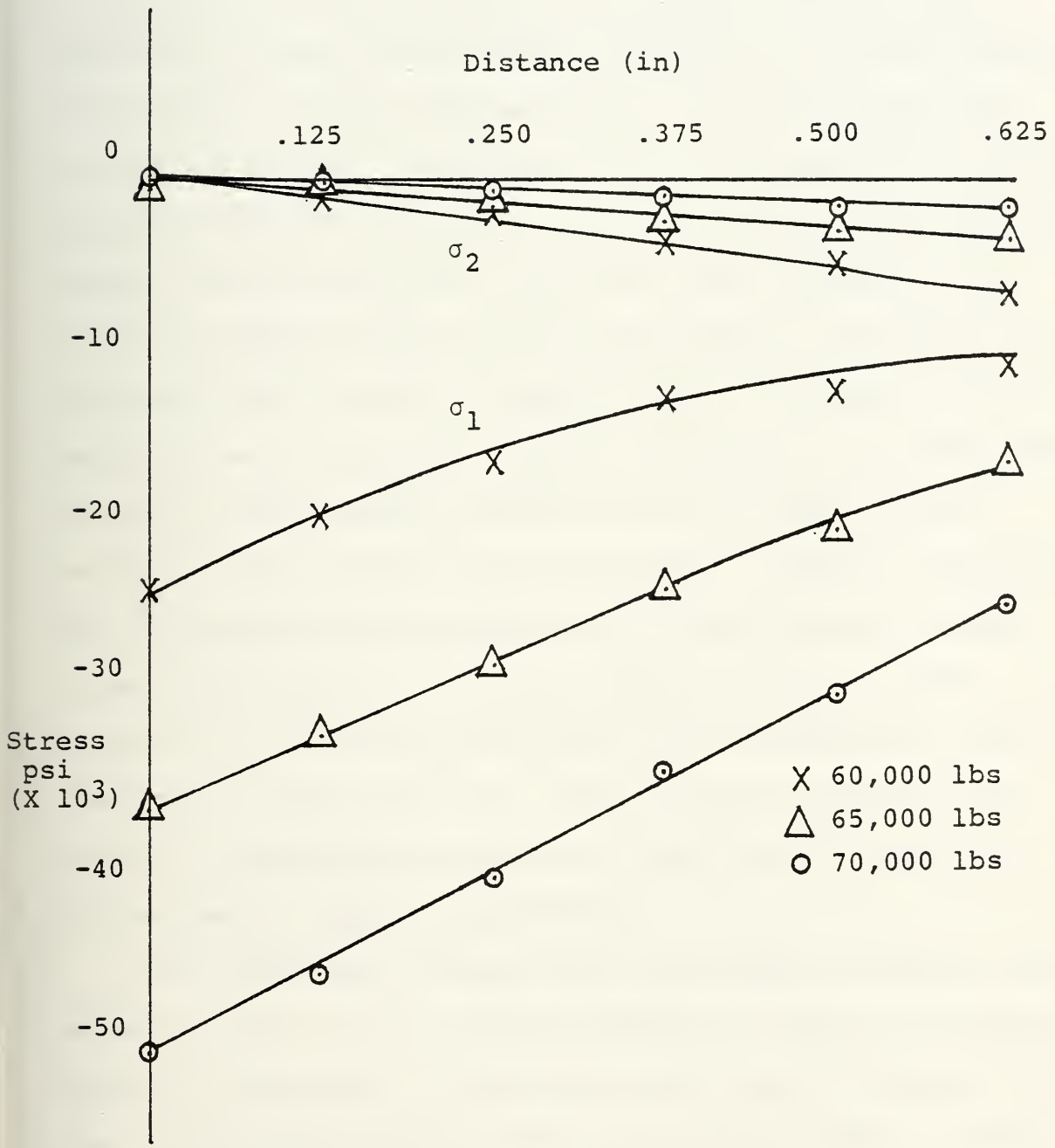

Figure 21

X. CONCLUSIONS

It has been clearly established that the photoelastic method of stress analysis can be accurate to within 2% by a comparison to the theoretical circular hole solution. Applying the same experimental methods to a notched specimen facilitated reliable evaluations of classical slip-line theory and Neuber's relation. Slip-line theory for a rigid-perfectly-plastic material indicated a gradual increase in stress levels beyond the tip, while data reduced by the modified Ramberg-Osgood method consistently exhibited the maximum stress levels at the notch tip. Although an error may have been introduced right at the notch tip by the over-sensitive photoelastic material used, the data did not exhibit erratic results in that region. Neuber's relation for the same region was applied at three separate stress levels and resulted in errors that varied very little. However, the level of the error, 20.9%, coupled with the results of Garske [Ref. 2], lead to the conclusion that methods of calculating stresses using Neuber's relation are subject to large inaccuracies.

This study also revealed the realities of working with materials that do not exhibit perfectly elastic or perfectly plastic properties. A transition zone exists between the two regions and creates difficulties in determining actual

plastic zone boundaries. Residual compressive stresses were present after a plastic region was produced with definite indications that the plastic zone at a yielded notch extends outward through strain levels that would be in the transition region of a uniaxial specimen.

APPENDIX A: EXPERIMENTAL DATA

TABLE I

PS-1C PHOTOELASTIC MATERIAL CHARACTERIZATION

σ psi	Net Reading	ε in/in	σ psi	Net Reading	ε in/in
0.0	0.0	0.0	0.0	0.0	0.0
202.37	2.76	0.000555	65.78	0.32	0.000064
408.42	5.74	0.001155	131.58	0.70	0.000141
610.26	8.47	0.001704	197.37	1.04	0.000209
785.26	11.02	0.002217	263.16	1.38	0.000278
990.53	14.80	0.002978	328.95	1.75	0.000352
1189.21	16.32	0.003284	394.74	2.08	0.000418
1407.63	19.38	0.003899	460.53	2.43	0.000489
1606.32	22.27	0.004481	526.32	2.76	0.000555

LINEAR REGRESSION:

$\sigma = 357079.18\varepsilon - 4.3407$ $\qquad$ $\sigma = 941487.02\varepsilon_2 + 1.00708$

$R = .9988$ $\qquad$ $R = .99991$

$\nu = .37927$

TABLE II

PS-1C F_σ DETERMINATION

σ psi	Compensator Reading	N
0.0	0.0	0.0
202.37	23.0	0.489
408.42	39.0	0.830
610.26	63.0	1.340
785.26	79.5	1.691
990.53	102.0	2.170
1189.21	123.0	2.617

LINEAR REGRESSION:

$\sigma = 456.6661N + 1.92740$

$R = .99932$

TABLE III

7075-T6 ALUMINUM CHARACTERIZATION

σ psi	ε_1 in/in	ε_2 in/in
12072.6	1138	-368
15090.8	1415	-465
18108.9	1710	-552
21127.1	1985	-650
24145.3	2290	-740
27163.4	2568	-838
30181.6	2880	-930
33199.7	3160	-1032
36217.9	3470	-1115
39236.0	3760	-1220

LINEAR REGRESSION:

$\sigma = 10.41518 \times 10^6 \varepsilon_1 + 242.076$

$R = .999921$

$\sigma = 32.19308 \times 10^6 \varepsilon_2 + 172.365$

$R = .999927$

$\nu = .32352$

TABLE IV

UNBOND CHARACTERISTICS OF PS-1C

Load lbs	Compensator Readings Unbond Specimen	Control Specimen
1027	20	18
1982	37	38
2990	55	56
3996	77	77
4997	99	101
5996	120	121
7008	144	146
8006	168	173
9001	188	192
10003	210	215
11001	231	237
12002	252	256
12999	274	282
13998	293	303
15001	312	328

TABLE V

CIRCULAR HOLE COMPENSATOR DATA

Data Point In.	Compensator Readings (corrected) C_n (Left/Right)	C_θ (Left/Right)
0.0	122.5/121.5	143.0/143.5
0.125	91.5/92.0	105.0/105.5
0.250	67.3/66.3	78.9/78.4
0.375	53.8/54.3	65.3/65.8
0.500	45.7/46.2	57.3/57.3

TABLE VI

CIRCULAR HOLE DATA COMPARISON

Data Point In.	$\sigma_{\theta/P}$	σ_θ psi	Experimental Stress Left	Right
0.0	3.24	34827	35188	35254
0.125	2.30	24723	24606	24672
0.250	1.85	19886	19644	19975
0.375	1.67	17951	17766	17832
0.500	1.54	16554	16786	16390

TABLE VII

CIRCULAR HOLE STRESSES AND STRAINS
FROM MEASURED DATA

Data Point In.	ε_1 10^{-3} in/in	ε_2 10^{-3} in/in	σ_1 psi	σ_2 psi
Left Side				
0.0	3.478	-1.119	35188	88
0.125	2.485	-0.948	24606	-1612
0.250	1.931	-0.594	19644	361
0.375	1.682	-0.337	17766	2350
0.500	1.542	-0.173	16786	3692
Right Side				
0.0	3.487	-1.129	35254	11
0.125	2.494	-0.958	24672	-1689
0.250	1.944	-0.543	19975	978
0.375	1.691	-0.347	17832	2273
0.500	1.520	-0.214	16390	3152

TABLE VIII

ELASTIC REGION LOADING

K_T = 3.8 Notch, 15,000 lb. Load

Data Pt. In.	Corrected C_n	Corrected C_θ	ε_1 10^{-3}in/in	ε_2 10^{-3}in/in	σ_1 psi	σ_2 psi
0.0	161.0	191.0	4.554	-1.488	45991	-141
0.125	94.5	120.6	3.320	-0.227	36668	9591
0.250	63.3	88.4	2.695	0.320	31613	13476
0.375	46.2	68.8	2.232	0.498	27036	13799
0.500	37.7	55.3	1.769	0.355	21283	10480
0.625	31.7	47.2	1.531	0.342	18544	9461
0.750	26.6	42.7	1.476	0.478	18425	10803

TABLE IX

ELASTIC REGION LOADING

K_T = 3.8 Notch, 20,000 lb. Load

Data Pt. In.	Corrected C_n	Corrected C_θ	ε_1 10^{-3}in/in	ε_2 10^{-3}in/in	σ_1 psi	σ_2 psi
0.0	213.0	253.0	6.041	-1.951	61098	68
0.125	131.7	161.8	4.238	-0.704	45293	7557
0.250	90.0	119.1	3.424	0.470	38850	13062
0.375	66.8	93.5	2.857	0.351	33558	14418
0.500	52.8	74.9	2.320	0.339	27447	12318
0.625	44.2	64.9	1.716	0.283	20423	9477

TABLE X

TRANSITION REGION LOADING

K_T = 3.8 Notch, 25,000 lb. Load

Data Pt. In.	Corrected C_n	Corrected C_θ	ε_1 10^{-3}in/in	ε_2 10^{-3}in/in	σ_1 psi	σ_2 psi
0.0	269.0	319.0	7.601	-2.493	76740	-336
0.125	157.3	193.5	5.077	-0.826	54328	9257
0.250	109.6	143.7	4.087	-0.256	46072	14668
0.375	81.4	113.1	3.430	0.376	40119	16795
0.500	64.8	90.5	2.759	0.328	32367	13800
0.625	54.3	75.4	2.285	0.248	26719	11161
0.750	48.2	65.8	1.959	0.150	22672	8861

TABLE XI

PLASTIC REGION LOADING

K_T = 3.8 Notch, 30,000 lb. Load

Data Pt. In.	Corrected C_n	Corrected C_θ	ε_1 10^{-3}in/in	ε_2 10^{-3}in/in	α_1 psi	σ_2 psi
0.0	319.0	378.5	9.025	-2.945	91172	-230
0.125	203.0	243.2	6.149	-1.469	64078	5913
0.250	138.2	172.4	4.609	-0.577	49949	10351
0.375	103.0	135.7	3.881	0.016	43903	14390
0.500	81.4	112.6	3.399	0.345	39656	16332
0.625	66.8	95.0	2.950	0.444	34946	15806
0.750	57.8	85.4	2.751	0.582	33200	16639

TABLE XII

ELASTIC REGION NORMALIZATION

K_T = 3.8 Notch, Elastic Region

Normalized to a 15,000 lb. Load

Data Pt. In.	Corrected C_n	Corrected C_θ	ε_1 10^{-3}in/in	ε_2 10^{-3}in/in	σ_1 psi	σ_2 psi
0.0	160.4	190.4	4.542	-1.476	45907	-45
0.125	96.6	121.0	3.252	-0.373	35372	7693
0.250	65.4	88.9	2.634	0.180	30410	11671
0.375	48.1	69.5	2.192	0.387	26177	12395
0.500	38.6	55.7	1.754	0.306	20939	9879
0.625	32.5	47.7	1.527	0.307	18373	9060
0.750	27.6	41.9	1.383	0.347	16891	8984

TABLE XV

ELASTIC REGION LOADING

K_T = 2.6 Notch, 10,000 lb. Load

Data Pt. In.	Corrected C_n	Corrected C_θ	ε_1 10^{-3}in/in	ε_2 10^{-3}in/in	σ_1 psi	σ_2 psi
0.0	62.0	73.5	1.751	-0.573	17696	-10
0.125	48.7	57.8	1.441	-0.386	14897	990
0.250	41.2	49.7	1.269	-0.277	13350	1584
0.375	34.7	42.2	1.090	-0.211	11562	1652
0.500	30.2	37.2	0.978	-0.155	10503	1878

TABLE XIV

ELASTIC REGION LOADING

K_T = 2.6 Notch, 15,000 lb. Load

Data Pt. In.	Corrected C_n	Corrected C_θ	ε_1 10^{-3}in/in	ε_2 10^{-3}in/in	σ_1 psi	σ_2 psi
0.0	93.0	110.5	2.639	-0.850	26749	190
0.125	73.4	86.9	2.159	-0.595	22252	1291
0.250	61.8	74.4	1.894	-0.425	19885	2236
0.375	52.3	63.3	1.624	-0.339	17142	2207
0.500	45.2	55.8	1.471	-0.225	15834	2926
0.625	41.2	50.3	1.306	-0.240	13909	2143

TABLE XV

ELASTIC REGION LOADING

K_T = 2.6 Notch, 20,000 lb. Load

Data Pt. In.	Corrected C_n	Corrected C_θ	ε_1 10^{-3}in/in	ε_2 10^{-3}in/in	σ_1 psi	σ_2 psi
0.0	124.0	147.0	3.501	-1.152	35391	-20
0.125	97.5	115.6	2.888	-0.780	29715	1871
0.250	82.4	99.5	2.544	-0.548	26793	3261
0.375	69.4	84.4	2.190	-0.424	23123	3304
0.500	60.3	74.4	1.960	-0.303	21085	3865
0.625	54.8	66.3	1.700	-0.356	17937	2288

TABLE XVI

PLASTIC REGION LOADING

K_T = 2.6 Notch, 60,000 lb. Load

Data Pt. In.	Corrected C_n	Corrected C_θ	ε_1 10^{-3}in/in	ε_2 10^{-3}in/in	σ_1 psi	σ_2 psi
0.0	431.0	511.0	12.173	-3.999	123060	-25
0.125	351.8	414.1	10.200	-3.001	104413	3946
0.250	295.5	351.8	8.813	-2.275	91403	7014
0.375	252.3	306.6	7.910	-1.557	83847	11800
0.500	216.1	263.3	6.818	-1.291	72460	10750
0.625	183.9	235.2	6.491	-0.409	72038	19520
0.750	162.3	207.1	5.700	-0.391	63134	16780
0.875	145.7	189.0	5.307	-0.160	59549	17940
1.000	132.2	174.9	5.027	0.066	57211	19460
RESIDUAL COMPRESSION						
0.0	83.5	99.0	-2.258	0.775	-23842	4
0.125	67.8	79.5	-1.947	0.597	-19837	-475
0.250	53.8	63.8	-1.589	0.430	-16409	-1044
0.375	39.2	47.2	-1.202	0.269	-12620	-1426
0.500	25.6	35.2	-1.056	-0.095	-12319	-5008
0.625	15.6	25.1	-0.869	-0.284	-10908	-6453

TABLE XVII

PLASTIC REGION LOADING

K_T = 2.6 Notch, 65,000 lb. Load

Data Pt. In.	Corrected C_n	Corrected C_θ	ε_1 10^{-3} in/in	ε_2 10^{-3} in/in	σ_1 psi	σ_2 psi
0.0	501.0	594.0	14.150	-4.649	143052	-23
0.125	411.1	480.4	11.700	-3.724	118751	1349
0.250	344.7	407.0	10.070	-2.863	103478	5038
0.375	293.5	352.8	8.963	-2.051	93935	10118
0.500	249.4	308.6	8.166	-1.189	88111	16920
0.625	215.1	272.4	7.425	-0.646	81740	20310
0.750	186.9	239.2	6.607	-0.406	73365	19990
0.875	165.8	212.1	5.855	-0.366	64993	17640
1.000	148.8	194.0	5.481	-0.103	61728	19230
RESIDUAL COMPRESSION						
0.0	128.0	152.0	-3.628	1.175	-36745	-191
0.125	112.6	131.6	-3.206	1.019	-32543	-387
0.250	93.5	110.6	-2.744	0.764	-28256	-1554
0.275	75.4	90.4	-2.288	0.541	-23914	-2381
0.500	61.3	74.3	-1.910	0.390	-20192	-2686
0.625	45.2	56.3	-1.502	0.194	-16300	-3392

TABLE XVIII

PLASTIC REGION LOADING

K_T = 2.6 Notch, 70,000 lb. Load

Data Pt. In.	Corrected C_n	Corrected C_θ	ε_1 10^{-3}in/in	ε_2 10^{-3}in/in	σ_1 psi	σ_2 psi
0.0	571.0	678.0	16.182	-5.244	163866	800
0.125	464.4	545.8	13.410	-4.014	137050	4426
0.250	393.9	472.4	11.960	-2.819	125057	12570
0.375	339.7	410.1	10.480	-2.264	110367	13360
0.500	294.5	361.8	9.476	-1.576	101522	17420
0.625	253.3	314.6	8.362	-1.143	90502	18160
0.750	219.1	281.4	7.807	-0.415	86927	24360
0.875	193.0	250.3	7.027	-0.215	78828	23710
1.000	170.9	225.3	6.436	0.024	73027	24220
RESIDUAL COMPRESSION						
0.0	178.0	211.0	-5.025	1.654	-50791	43
0.125	158.8	185.8	-4.535	1.424	-46086	-736
0.250	139.7	163.7	-4.004	1.238	-40774	-878
0.375	117.6	138.1	-3.389	1.023	-34600	-1016
0.500	100.5	118.5	-2.926	0.845	-30017	-1316
0.625	81.4	96.5	-2.402	0.652	-24798	-1551

TABLE XIX

MODIFIED RAMBERG-OSGOOD STRESSES

K_T = 2.6 Notch, 60,000 lb. Load

Data Point In.	σ_1 psi	σ_2 psi
0.0	77245	-690
0.125	75623	3372
0.250	73913	6503
0.375	72460	11311
0.500	68752	10326
0.625	68526	19088
0.750	62501	16409
0.875	59207	17580
1.000	56473	17614

TABLE XX

MODIFIED RAMBERG-OSGOOD STRESSES

K_T = 2.6 Notch, 65,000 lb. Load

Data Point In.	σ_1 psi	σ_2 psi
0.0	78463	-808
0.125	76922	687
0.250	75520	4455
0.375	74303	9580
0.500	73332	16402
0.625	71942	19826
0.750	69139	19551
0.875	64037	17254
1.000	61237	18861

TABLE XXI

MODIFIED RAMBERG-OSGOOD STRESSES

K_T = 2.6 Notch, 70,000 lb. Load

Data Point In.	σ_1 psi	σ_2 psi
0.0	79426	-104
0.125	78132	3659
0.250	77379	11855
0.375	76206	12716
0.500	75291	16828
0.625	73754	17637
0.750	73097	23835
0.875	71129	23237
1.000	68978	23775

TABLE XXII

NEUBER'S RELATION COMPARISON, $K_T = 2.6$

σ_{nom} psi	σ_1 psi	ε_1 10^{-3} in/in	K_T	% Error
31915	77245	12.173	9.33	21.2
34575	78463	14.150	9.39	20.6
37234	79426	16.182	9.37	20.8

Neuber's Equivalent K_T 3.44 (far-field)

$K_T^2 = 11.83$

$$K_T^2 = \frac{\sigma_1 E \varepsilon_1}{\sigma_{nom}^2}$$

LIST OF REFERENCES

1. Neuber, H., "Theory of Stress Concentration of Shear Strained Prismatic Bodies with Arbitrary Nonlinear Stress-Strain Law," Journal of Applied Mechanics, December 1961.

2. Garske, J. C., An Investigation of Methods for Determining Notch Root Stress from Far-Field Strain in Notched Flat Plates, Master's Thesis, Naval Postgraduate School, Monterey, California, September 1977.

3. Topper, T. H., Wetzel, R. M., and Morrow, J., "Neuber's Rule Applied to Fatigue of Notched Specimens," Journal of Materials, March 1969.

4. Schijve, J., The Accumulation of Fatigue Damage in Aircraft Materials and Structures, paper presented at the Symposium on Random Load Fatigue, Lyngby, Denmark, 13 April 1972.

5. Rotvel, F., On Residual Stresses During Random Load Fatigue, paper presented at the Symposium on Random Load Fatigue, Lyngby, Denmark, 13 April 1972.

6. Aminco-Tuckerman Optical Strain Gage System Instructions No. 750, p. 16, American Instrument Company, Inc., 1958.

7. Zandman, F., Redner, S., and Dally, J. W., Photoelastic Coatings, The Iowa State University Press and Society for Experimental Stress Analysis, 1977.

8. Howland, R. C. J., "Stresses in a Strip of Finite Width Which is Weakened by a Circular Hole," Philosophical Transactions of the Royal Society, Series A, V. 229, p. 49, London, 1930.

9. Stuart, G. L., An Investigation of Residual Stress Characterization of 7075-T6 Aluminum for Application in Fatigue Analysis, Master's Thesis, Naval Postgraduate School, Monterey, California, December 1978.

10. Engle, E. C., An Investigation of Residual Stresses in Simulated Wing Panels of 7075-T6 Aluminum, Master's Thesis, Naval Postgraduate School, Monterey, California, December 1979.

11. Kim, Y. H., Fine, M. E., and Mura, T., Plastic Yielding at the Tip of a Blunt Notch During Static and Fatigue Loading," Engineering Fracture Mechanics, V. 2, p. 653, Pergamon Press, Ltd., 1979.

12. Kachanov, L. M., Foundations of the Theory of Plasticity, Translated from the Russian by Multilingual Scientific Translations, p. 127, North Holland Publishing Company, 1971.

INITIAL DISTRIBUTION LIST

		No. Copies
1.	Defense Technical Information Center Cameron Station Alexandria, Virginia 22314	2
2.	Library, Code 0142 Naval Postgraduate School Monterey, California 93940	2
3.	Department Chairman, Code 67 Department of Aeronautics Naval Postgraduate School Monterey, California 93940	1
4.	Professor G. H. Lindsey, Code 67Li Department of Aeronautics Naval Postgraduate School Monterey, California 93940	1
5.	LCDR Frank E. Stenstrom, USN 3365 Glen Eden Quay Virginia Beach, Virginia 23452	1